Modes of micromolar host-guest binding of beta-cyclodextrin complexes revealed by NMR spectroscopy in salt water

Modes of micromolar host–guest binding of β-cyclodextrin complexes revealed by NMR spectroscopy in salt water

Josef Tomeček,[a] Andrea Čablová,[a] Aneta Hromádková,[a] Jan Novotný,*[b,c] Radek Marek,[b,c,d] Ivo Durník,[b,c] Petr Kulhánek,*[b,c] Zdeňka Prucková,[a] Michal Rouchal,[a] Lenka Dastychová,[a] and Robert Vícha*[a]

[a] Department of Chemistry, Faculty of Technology, Tomas Bata University in Zlín, Vavrečkova 275, 760 01 Zlín, Czech Republic. E-mail: rvicha@utb.cz; Tel: +420-576031103

[b] CEITEC – Central European Institute of Technology, Masaryk University, Kamenice 5, 625 00 Brno, Czech Republic. E-mail: kulhanek@chemi.muni.cz; Tel: +420-549495459 (P. Kulhánek). E-mail: jan.novotny@ceitec.muni.cz; Tel: +420-549496440 (J. Novotný).

[c] National Centre for Biomolecular Research, Faculty of Science, Masaryk University, Kamenice 5, 625 00 Brno, Czech Republic.

[d] Department of Chemistry, Faculty of Science, Masaryk University, Kamenice 5, 625 00 Brno, Czech Republic.

Table of Contents graphics

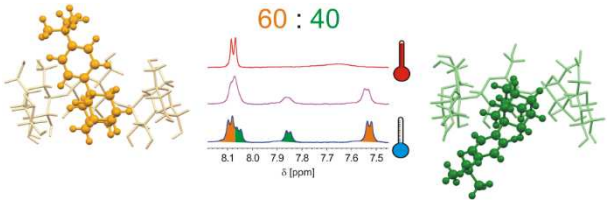

Abstract

Multitopic supramolecular guests with finely tuned affinities towards widely explored cucurbit[*n*]urils (CB*n*s) and cyclodextrins have been recently designed and tested as functional components of advanced supramolecular systems. We employed various spacers between the adamantane cage and a cationic moiety as a tool for tuning the binding strength towards CB7 to prepare a set of model guests with K_{CB7} and $K_{\beta\text{-CD}}$ values of (0.6–5.0)×10^{10} M^{-1} and (0.6–2.6)×10^{6} M^{-1}, respectively. These accessible adamantylphenyl-based binding motifs open a way towards supramolecular components with an outstanding affinity towards β-cyclodextrin. ^{1}H NMR experiments performed in 30% $CaCl_2/D_2O$ at 273 K along with molecular dynamics simulations allowed us to identify two arrangements of the guest@β-CD complexes. The approach, joining experimental and theoretical methods, provided a better understanding of the structure of cyclodextrin complexes and related molecular recognition, which is highly important for the rational design of drug delivery systems, molecular sensors and switches.

Keywords

cucurbit[*n*]urils; cyclodextrins; host–guest systems; molecular dynamics; NMR spectroscopy

Introduction

Cyclodextrins (CDs) and cucurbit[*n*]urils (CBs) are two families of supramolecular macrocyclic hosts, which can bind guest molecules into their cavities. Because of the comparable size of their interior

cavities, corresponding homologues bind guests of similar size and shape.[1] However, the binding strength can differ significantly. Whereas the hydrophobic effect and hydrogen bonds are the main binding forces in both families, they can be accompanied by ion–dipole interactions in the case of CBs.[2] The highest affinity towards CDs was observed for derivatives of cage diamondoids, which perfectly fit their cavities. For example, the value of association constant for 1:1 complex of triamantane-9-carboxylic acid and β-CD reaches the order of 10^6 M^{-1} (carbonate buffer, pH=10.5, 298 K).[3] The presence of a positive charge in the guest molecule usually plays a marginal role in the binding by unmodified CDs. In contrast, if lipophilic cages like adamantane,[4] diamantane,[5] bicyclo[2.2.2]octane,[4a] cubane[6] or ferrocene[7] are decorated with cationic moieties, outstanding binding strengths with geometrically complementary CBs can be achieved. For example, 4,9-bis(trimethylammonio)diamantane forms the tightest 1:1 host–guest complex with CB7 (K=7.2×10^{17} M^{-1} in D_2O) that has ever been reported.[5a]

Analysing binding data of an extensive series of complexes, as Nau did in his review in 2015,[2] the individual contributions of the hydrophobic effect and ion–dipole interactions can be quantified as follows: whereas the hydrophobic effect with the release of high-energy water molecules from the CB cavity and desolvation of the guest surface can account for an association constant as high as 10^{10} to 10^{12} M^{-1}, the strength of ion–dipole interactions is much lower and adds a factor of up to 10^3 for one cation–portal interaction.

Another feature of inclusion complexes between CB7 and adamantane derivatives is their tight fit. As a result, the adamantane cage cannot move significantly from the optimal position inside the cavity[8] contrary to derivatives of linear aliphatic hydrocarbons[9] as has been indicated by molecular dynamic simulations.[10] Because adamantane-based ligands are tightly anchored within the complex and ion–dipole interactions between the cationic part of the guest and the CB7 portal cannot surpass the hydrophobic forces,[8] the contribution of the ion–dipole interaction should be easily adjusted by changing the length of a rigid linker between adamantane cage and the cationic part. Values of association constants can then, theoretically, range from 10^8 to 10^{15} M^{-1}. These values were reported for adamantane derivatives with a long non-charged chain in the position one[10] or even for anionic complexes of Ru(III)[8] and singly positively charged adamantane derivatives with a cationic part in the optimal position,[4a] respectively.

The design of multitopic guests is an intriguing challenge as resulting supramolecular assemblies can be used for catalysis, drug delivery and release[11] or sensor preparation.[12] For example, Yan and co-workers have recently prepared a rotaxane molecular reactor consisting of a biphenyl axle, modified γ-CD and two CB6 stoppers.[13] This system catalyses photoisomerisation of (*Z*,*Z*)-1,3-cyclooctadiene to (*Z*,*E*)-1,3-cyclooctadiene with an enantiomeric excess of up to 15.3%. In extension of a pioneering work in the eighties of the last century,[14] a number of supramolecular systems based on multitopic guest have been recently reported to demonstrate importance of lateral interactions between adjacent macrocycles[15] or switching the arrangements upon chemical signals.[16]

As a part of our ongoing research on a multitopic guests, we developed binding motifs with precisely tuned binding strengths towards CBs and CDs. In this study, we report a series of adamantane-based guests with a cationic moiety linked via the benzene ring. We expected a medium binding strength (i.e. K_{CB7}≈10^{10} M^{-1}) towards cucurbit[7]uril (CB7) and essentially unaffected binding into β-CD (i.e. $K_{\beta\text{-CD}}$≈10^5 M^{-1}). Surprisingly, the observed affinities of our new ligands towards β-CD were of 10^6 M^{-1} attacking the strongest 1:1 complexes of β-CD reported so far.[3] In addition, we found that there are two distinct binding modes in the aqueous solution. As cyclodextrin complexes usually display binding in a fast exchange regime, obtaining geometry of the complexes is troublesome. In this account, we introduce a new methodology, joining low-temperature NMR and molecular modelling, overcomes these limitations and allows for the better-targeted design of supramolecular systems.

Results and discussion

Chemistry

The nature of cationic moiety has an important impact on supramolecular properties of the guests. Tetraalkylammonium, alkylpyridinium and dialkylimidazolium salts are the most popular cationic species extensively studied in supramolecular chemistry. Therefore, we prepared five model guests to represent all these classes of compounds. We started from commercially available 1-bromoadamantane (**1**), which was reacted with toluene in the presence of Lewis acid (Scheme 1). It was previously demonstrated that *meta*-derivative is formed from *para*-derivative via subsequent rearrangement catalysed by Lewis acids.[17] Therefore, we employed two types of Lewis acids, $InCl_3$ and $AlCl_3$, to achieve a significantly different ratio of *para* and *meta* regioisomers of 1-adamantyltoluenes

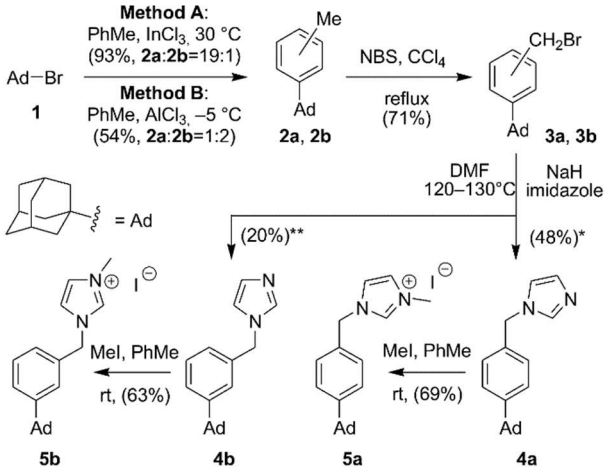

Scheme 1 Synthesis of guests **5a** and **5b**. Isolated yields are given in brackets. * and ** indicate that the reaction was started from a **2a**:**2b** mixture of 19:1 and 1:2, respectively.

2a and **2b**. Due to similar chemical properties of regioisomers, the mixture of **2a** and **2b** was used in the next bromination step without separation. Similarly, the bromoderivatives **3a** and **3b** were not separated. However, a single crystal of **3b** was obtained from an oily mixture of both isomers to allow unambiguous structure determination using NMR and X-ray diffraction (Figure S41, Table S1). Subsequently, a mixture of **3a** and **3b** was treated with sodium imidazolide in DMF and obtained imidazoles **4a** and **4b** were separated using repeated column chromatography. It is worth noting that isolated yields of pure imidazoles **4** can be improved using a more efficient separation system or by further purification of mixed portions since the conversion of **3** to **4** was quantitative, according to GC–MS and TLC. Finally, imidazoles **4a** and **4b** were methylated by MeI to yield imidazolium salts **5a** and **5b**. The structure of **5b** was verified by a single-crystal X-ray diffraction analysis (Figure S42, Table S1).

Additional three guests were synthesised via intermediate 4-(1-adamantyl)aniline (**8**), which was readily prepared from **1** via Friedel–Crafts alkylation of benzene, nitration and reduction, as can be seen in Scheme 2. The third imidazolium-derived guest **10**, in which the imidazole core is directly linked to the benzene ring, was prepared according to a one-pot, four-component methodology and subsequent methylation by MeI (Scheme 2). The imidazole formation step was not optimised. Trimethylammonium salt **11** was prepared via a conventional methylation approach under mild basic conditions. Finally, pyridinium salt **12** was obtained via the Zincke reaction.[18] Preparation of analogous triflate salt of **12** was recently reported.[19] However, the *para* derivative was accompanied by a significant portion of *ortho* (33%) and *meta* (47%) isomers, and the authors did not separate them. Before further use, all salts were dried in a vacuum (<1 torr, 30 °C) and stored under argon atmosphere.

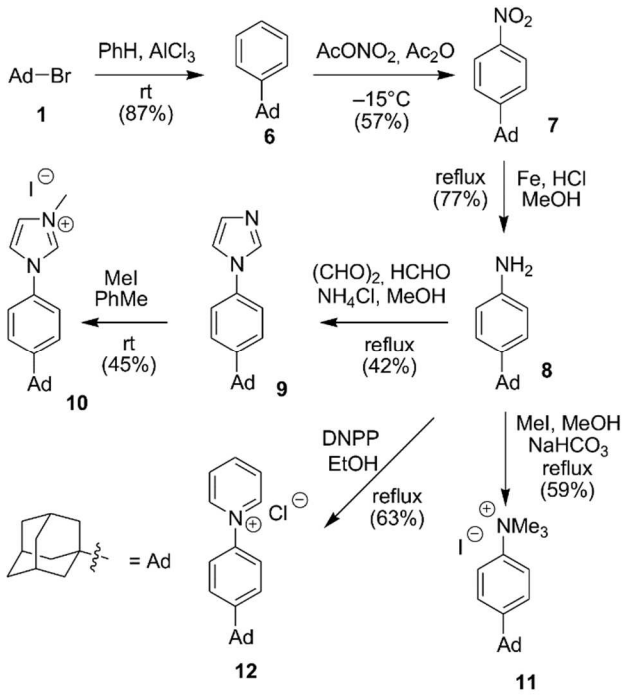

Scheme 2 Synthesis of guests **10**–**12**. Isolated yields are given in brackets. DNPP = *N*-(2,4-dinitrophenyl)pyridinium chloride.

Titration calorimetry

Because the determination of binding affinities of the new guests towards CB7 and β-CD was the initial intention of this work, we employed titration calorimetry (ITC) to obtain detailed thermodynamic information regarding studied systems.

Recently, we reported binding constants for two imidazolium-based guests with CB7.[10] The first guest with a short methylene linker between the adamantane cage and imidazolium moiety displayed a binding constant K of 3.68×10^{12} M^{-1}. In contrast, the second guest with a longer linker (oxo-*p*-xylylene) displayed $K=2.69\times10^{8}$ M^{-1}. We also demonstrated that the contribution of the ion–dipole interaction to the complex stabilisation in the case of the latter guest is very weak if any. The highest affinity of singly charged adamantane derivative towards CB7 was reported for 1-adamantylmethylammonium ($K=7.58\times10^{14}$ M^{-1}),[20] and other common derivatives carrying a single positive charge displayed K in the order of 10^{12} M^{-1} ($AdN^+Me_3I^-$ $K=1.71\times10^{12}$ M^{-1}, $AdN^+H_3Cl^-$ $K=4.23\times10^{12}$ M^{-1}, $AdPy^+Br^-$ $K=1.98\times10^{12}$ M^{-1}).[4b] We assumed that linkers shortened by one (guests **5a** and **5b**) or by two methylene bridges (guests **10**–**12**) in comparison to the abovementioned guest with the oxo-*p*-xylylene linker allow more efficient involvement of the ion–dipole interaction to provide guests with intermediate binding strengths towards CB7. The obtained results are summarised in Table 1 (see Figures S34–S38 for detailed titration data). All five examined guests show a binding strength towards CB7 in the order of 10^{10} M^{-1}. Small differences in affinities correlate with the distance between the cationic moiety and the adamantane cage. Thus, the guest **5a** with the most extended spacer displays the lowest K value, whereas guests **11** and **12** with cationic moiety directly bound to the phenyl ring display the highest affinities towards CB7. The correlation of binding affinity (K) vs linker length between adamantane and ammonium moiety is shown in Figure S39.

Generally, binding strengths of CDs are significantly lower than those of CBs due to higher flexibility and a lack of specific (e.g. ion–dipole) interactions. Complexes of CDs with K values in order of 10^5 M^{-1} are usually considered as very stable. To our best knowledge, the strongest complex of β-CD was recently reported by Schibilla and co-workers, who described the binding behaviour of triamantane-9-

carboxylic acid.[3] This compound and β-CD subsequently form 1:1 and 1:2 complexes with K_1=2.95×10^6 M^{-1} and K_2=1.4×10^4 M^{-1}.

Table 1 Thermodynamic parameters obtained by ITC in H_2O at 303 K.

Guest	Host	*n*	*K* [dm^3·mol^{-1}]	Δ*H* [kJ·mol^{-1}]	−*T*Δ*S* [kJ·mol^{-1}]	Δ*G* [kJ·mol^{-1}]
5a	CB7	1.00 ± 0.08	(6.1 ± 1.4)×10^9 [a]	−81.7 ± 1.6	24.9 ± 1.5	−57 ± 2
	β-CD	1.07 ± 0.04	(2.61 ± 0.11)×10^6	−39.99 ± 0.04	2.76 ± 0.01	−37.23 ± 0.10
5b	CB7	1.02 ± 0.05	(2.3 ± 0.6)×10^{10} [a]	−88 ± 2	28 ± 2	−60 ± 2
	β-CD	1.01 ± 0.03	(4.05 ± 0.17)×10^5	−36.1 ± 0.8	3.6 ± 0.7	−32.54 ± 0.10
10	CB7	0.84 ± 0.05	(3.1 ± 0.7)×10^{10} [a]	−83.0 ± 1.5	22.1 ± 1.4	−61 ± 3
	β-CD	0.98 ± 0.01	(8.53 ± 0.13)×10^5	−36.5 ± 0.4	2.1 ± 0.4	−34.42 ± 0.04
11	CB7	0.97 ± 0.11	(3.4 ± 0.8)×10^{10} [a]	−80.8 ± 1.3	19.7 ± 1.2	−61 ± 3
	β-CD	0.98 ± 0.03	(7.9 ± 0.2)×10^5	−35.8 ± 1.7	1.6 ± 1.7	−34.22 ± 0.07
12	CB7	1.05 ± 0.05	(4.7 ± 1.9)×10^{10} [a]	−76.4 ± 0.8	14.1 ± 1.0	−62 ± 3
	β-CD	1.06 ± 0.01	(6.4 ± 0.7)×10^5	−33.3 ± 0.5	−0.4 ± 0.5	−33.71 ± 0.02

[a] 1-hexyl-3-methylimidazolium chloride was used as a competitor

Interestingly, all of our new guests displayed unexpectedly high affinities towards β-CD within the range of (0.4–2.6)×10^6 M^{-1}. In comparison with CB7, the trend of *K* value dependency on the linker length is opposite in the case of β-CD complexes (Figure S39). The guest **5a** with the longest spacer provided the highest affinity towards β-CD and vice versa. The guest **5b** stands apart from this trend most likely due to its bent structure, which does not allow for deeper guest burying into the β-CD cavity. Interestingly, NMR experiments revealed two distinct 1:1 binding modes for all examined guests with β-CD. Therefore, the *K* values reported in Table 1 should be understood as apparent association constants averaging the *K* values of all complexes, which are populated in equilibria.

As seen in Table 1, formation of all examined complexes was driven by enthalpic gain, which was accompanied by an entropic penalty. Figure S40 shows enthalpy–entropy scatter plot for our complexes in the context of previously described high-affinity complexes of CB7[4a] and comprehensive set of cyclodextrin complexes reported by Inoue and Rekharsky.[1b] Data of our CB7–guest pairs appear consistently within the set of the previously published systems which are known for their ability to overcome the usual enthalpy–entropy compensation pattern. In comparison to the previously published β-CD data set, the lower absolute value of the slope α and larger intercept −*T*Δ*S*$_0$ indicate lower influence of conformational changes and the greater desolvation, respectively.

Mass spectrometry

The ability of all prepared guests to form supramolecular complexes with β-CD and CB7 was also studied using mass spectrometry. The equimolar mixtures of the guest and host, and 1:3 mixture of guest **12** and β-CD, were prepared immediately before each measurement. In the first-order mass spectra of all studied mixtures, the signals, which can be attributed to complexes with 1:1 stoichiometry, were observed. These signals were accompanied by signals of singly charged ions related to the corresponding guests. Additionally, adducts of singly charged sodium and potassium with β-CD and doubly charged calcium adduct with two CB7 were also observed in the spectra (Figures S51–S60). The gas-phase behaviour of the complexes was studied using collision-induced dissociation (CID) after isolation of the required ion. Nevertheless, the fragmentation was successful only in the case of mixtures of guests **5a**, **5b** and **11** with CB7. As can be seen from MS/MS spectra, the gas-phase behaviour of complexes **5a**@CB7 and **5b**@CB7 was similar (Figures S56, S57). Under the CID conditions, the neutral loss of 1-methylimidazole from the guest molecule led to the formation of the singly charged ion observed at *m/z* 1387, which can be rationalised as a corresponding benzyl cation

complexed with CB7. Moreover, singly charged CB7 without a single hydrogen atom (*m/z* 1161) was observed in both tandem mass spectra as the most abundant product ion. Suggested fragmentation pathway is given in Scheme S1. The ability of CB7 to act as a hydride donor in the reaction with similar benzyl cations was described in detail in our previous work.[21]

NMR results

Simultaneous to ITC and MS measurements, we performed ^{1}H NMR titrations to obtain additional information about complex formation. All examined guests bind CB7 in a slow-exchange mode as monitored by NMR spectroscopy. As can be seen in Figures S27–S31, a new subset of signals for adamantane H-atoms appeared at lower values of a chemical shift, whereas original signals diminished when the molar fraction of CB7 exceeded 0.5. In concert with the ITC results, this can be explained by the formation of 1:1 complexes with the adamantane cage encapsulated into the CB7 cavity. Because preliminary experiments indicate fast complexation regime in the case of β-CD, we confirmed 1:1 stoichiometry of the complexes by Job's approach[22] prior to titration experiments (see Figures S32 and S33). Titrating our guests with β-CD, we observed the most significant changes in the NMR resonance area of the adamantane signals. As these signals moved to higher frequencies, we infer that the adamantane cage was positioned inside the β-CD cavity in all cases. Results are given in Figures S19–S23. However, we observed unexpected selective broadening of some signals during the experiments with β-CD. The titration experiment of **11** with β-CD is shown in Figure 1 as an example. The signals of H_d and H_{ax} became significantly broad when the amount of β-CD in the mixture exceeded one equivalent (compare 0.8 and 1.2 eq. in Figure 1). Note that signals of the host H-atoms located inside the β-CD cavity were broadened as well (Figure 1, Figure S22).

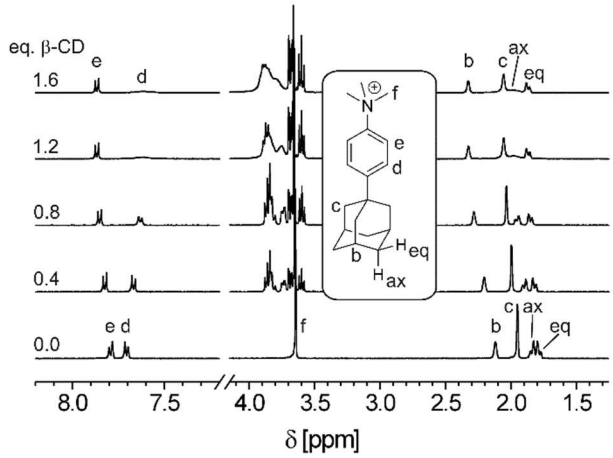

Figure 1 Portions of ^{1}H NMR spectra recorded during titration of the guest **11** (bottom line) by β-CD (D_2O, 303 K).

Subsequently, we analysed other titration data to observe the same pattern. In the case of all examined guests, signals of H-atom at the phenylene ring adjacent to the adamantane cage and the H-atom in the axial position on the unsubstituted cyclohexane ring of the adamantane cage were broadened (Figure 2). Because this behaviour was observed for all five new guests, we decided to examine this phenomenon in more detail. One of our initial hypotheses was that there is an equilibrium of at least two distinct supramolecular arrangements in a moderate-exchange manner. Therefore, we recorded ^{1}H NMR spectra at various temperatures. While increased temperature caused only insignificant sharpening of the signals (spectrum of **5a**@β-CD recorded at 323 K is shown in Figure S19, top line), we clearly observed the splitting of the guest H_d signal in the spectrum of an equimolar mixture of **11** and β-CD at 278 K (Figure 3, line ii). However, these signals were still too broad, and

other signals were not resolved at all. Therefore, we tested other approaches to allow recording spectra at a lower temperature. These tests were performed only with the guest **11** due to its simple ^{1}H NMR spectrum. Initially, we tried mixtures of water and DMSO. It is well known that DMSO/water mixtures display extreme deviations from additivity, and a very low freezing point 133 K was measured at DMSO molar fraction of 0.33.[23] Unfortunately, we did not find any portion of DMSO, which would allow for both the measurements below 273 K and the observation of the two resolved sets of signals.

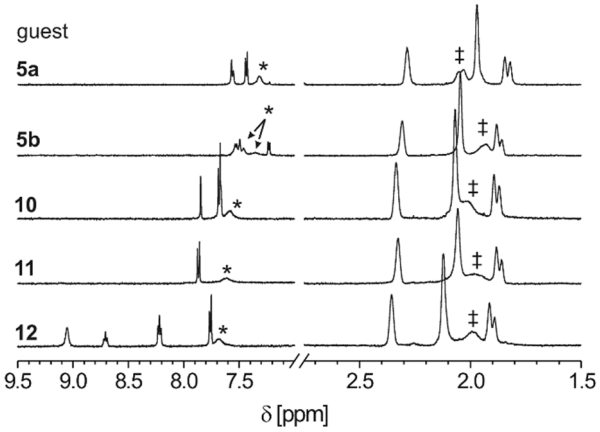

Figure 2 Portions of ^{1}H NMR spectra of 2:3 mixtures of the guests and β-CD (D_2O, 303 K). Signals of phenyl hydrogen atoms in the *ortho* positions to 1-adamantyl are asterisked. Signals of adamantane H-atoms in the axial positions (see Figure 1) are assigned with ‡.

Subsequently, we recorded the ^{1}H NMR spectra in a 30% solution of $CaCl_2$ in D_2O with 5 K steps. Even at 303 K (Figure 3, line iii), better separation of signals than that in pure D_2O at 278 K was observed. Additional decreasing of the temperature further improved the separation of all guest signals. We observed the sharpest peaks and best signal separation at 273 K. Subsequent decrease of the temperature led to slight signal broadening while no progress in signal separation was observed. Finally, we measured the same mixture at 950 MHz at 273 K to achieve the perfect resolution of the two sets of signals (Figure 3, line iv).

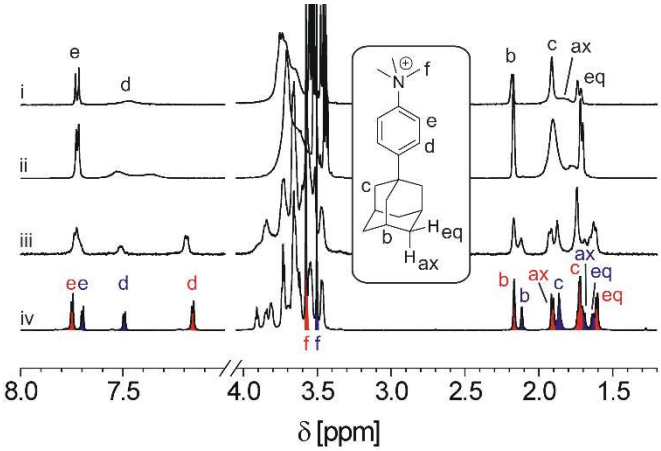

Figure 3 Portions of ^{1}H NMR spectra of a 1:1 mixture of guest **11** and β-CD: i) D_2O, 303 K, 500 MHz; ii) D_2O, 278 K, 700 MHz; iii) 30% $CaCl_2$ in D_2O, 303 K, 700 MHz; iv) 30% $CaCl_2$ in D_2O, 273 K, 950 MHz, the red and blue colour indicates the **NP** and **NS** complex, respectively (for representative supramolecular structures of host–guest complexes, see Figure 5).

Thus, we conclude that these low-temperature NMR results strongly support the presence of two distinct geometrical arrangements of the complexes of our new guests with β-CD. We suggest that two binding arrangements differ in the orientation of **11** inside of the β-CD cavity. In the first orientation, denoted as **NP**, the ammonium part (with nitrogen [N]) of **11** points towards the primary (P) rim of β-CD, whereas in the second one, denoted as **NS**, the ammonium part aims at the secondary (S) rim. The **NS**/**NP** ratio of 40/60 was estimated at 273 K using the integration of the spectrum iv in Figure 3. Assignment of NMR signals of suggested binding forms based on molecular modelling and ^{1}H–^{1}H NOESY experiments will be thoroughly discussed in the following sections.

We also estimated the experimental value of rate constant and activation free energy barrier for the **NS**↔**NP** interconversion of the **11**@β-CD complex in 30% $CaCl_2$ from temperature-dependent measurements at 500 MHz NMR spectrometer. If we neglect slightly different populations of both states, the rate constant of interconversion can be determined approximatively in the intermediate exchange range at the coalescence temperature.[24] The coalescence temperature was determined from a measurement, in which two separate peaks merged into a flat-topped peak. The coalescence occurred at 350 and 310 K (with a resolution of about 5 K) for well-resolved aromatic H_d and H_e protons of guest **11**, respectively. Observed separation of H_d and H_e signals in the slow-exchange regime were 0.33 and 0.04 ppm, which provided the following rate constants: 367 s^{-1} at 350 K and 44 s^{-1} at 310 K. Finally, the activation free energy barriers obtained by applying the Eyring equation were determined as 69.0 and 66.2 kJ·mol^{-1}, respectively.

Molecular dynamic simulation of 11@β-CD

NMR observations suggested that the timescale for interconversion between two forms of **11**@β-CD complex (≈ms) is beyond the possibilities of regular molecular dynamic (MD) simulations (≈μs). Thus, we employed biased adaptive biasing force/multiple walker (ABF/MWA) simulations, allowing us to sample all possible arrangements of **11** and β-CD in a reasonable computational time (see Computational methods and Supporting Information). Using two collective variables (Figure S61) for the description of the mutual position (d_{ODIS}) and orientation (α_{PVANG}) of **11** and β-CD, we got the free energy surface shown in Figure 4A.

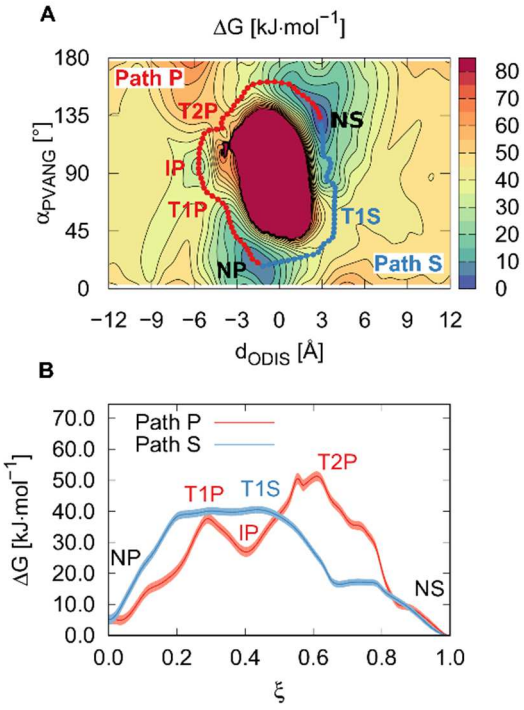

Figure 4 A) Calculated free energy surface as a function of two collective variables d_{ODIS} and α_{PVANG} (Figure S61). Suggested binding modes correspond to the free energy minima **NP** and **NS**, which are connected by two minimum free energy pathways. **IP** is an intermediate (local free energy minimum), and **T1P**, **T2P**, **T1S** are transition states (saddle points) along the pathways. Isolines are spaced by 5 kJ·mol^{-1}. B) Minimum free energy pathways extracted from the free energy surface representing interconversion of **NP** to **NS**. Path P shows interconversion occurring at the side of the primary portal, while Path S is at the secondary portal. **IP** is an intermediate on Path P**,** and **T1P**, **T2P**, **T1S** are transition states (see Table S8 for their summary). ξ is a dimensionless parameter describing positions along the paths. Confidence intervals (errors) of calculated free energies are shown as light colour strips at three standard deviations.

Two suggested binding modes, **NP** and **NS**, appeared as local minima on the calculated surface. The calculation indicated that the state **NP** could not be simply converted to **NS** through rotation of **11** inside the cavity, as this process would result in the enormous rise of the free energy (see the red part around d_{ODIS}≈0 Å in Figure 4A). Instead, there are two possible interconversions represented as two minimum free energy pathways connecting **NP** and **NS** (Figure 4B, Table S8). While **11** dissociates on the side of the primary rim along Path P, it leaves the cavity at the side of the secondary rim along Path S. Additionally, Path P features one extra free energy minimum (intermediate IP). Representative structures belonging to important thermodynamic states were extracted from ABF/MWA trajectories and are depicted in Figure 5. In accordance with ^{1}H NMR experiments, both **NP** and **NS** have the adamantane cage inside the cavity, while the rest of the guest is located outside the macrocycle. In the case of **NP**, the phenyltrimethylammonium arm is on the primary side of β-CD, while it is on the secondary side of β-CD in **NS**. In addition, we found an intermediate IP, which captures **11** bound outside the β-CD cavity. The structure of IP shows a parallel alignment of **11** with the β-CD plane and interaction with the primary portal of β-CD.

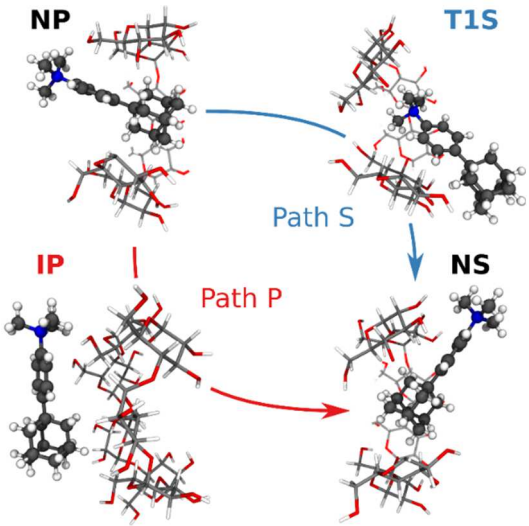

Figure 5 Representative structures along two possible interconversion pathways from **NP** to **NS**. Guest **11** is represented in dark grey, β-CD in light grey, O-atoms in red, N-atoms in blue.

The obtained free energy surface exhibits only a qualitative thermodynamic agreement with the experiment. The calculation suggests that **NS** is more stable than **NP** ($\Delta G_{\mathrm{NS-NP}} = -5.1 \pm 1.5$ kJ·mol^{-1} at 300 K, *c*(NaCl) = 0.14 M), while NMR showed it the opposite ($\Delta G_{\mathrm{NS-NP}} = +1.2$ kJ·mol^{-1} at 273 K, *c*($CaCl_2$)≈3.4 M). However, the difference between **NS** and **NP** was found to be small in both cases, which indicates that two states would be similarly populated, as observed experimentally. The

difference is most likely caused by inaccurate force field parameters and different environmental conditions than in the experiment (low temperature and high salt concentration).

Most importantly, no other stable complex arrangements than **NP** and **NS** were detected by extensive ABF/MWA sampling. The estimated population of IP from calculated data is 0.002% at 300 K, indicating that IP would be barely detectable by NMR. The size of barriers along both pathways suggests that Path S is likely to be the preferred way of the interconversion with a rate-limiting step of 41.0 kJ·mol^{-1}, compared to Path P with the highest transition state at 51.9 kJ·mol^{-1}. Barriers obtained from the modelling are underestimated in comparison to the experimentally determined value (≈68 kJ·mol^{-1}). Apart from the inaccuracies of the employed empirical force field, the most significant impact on the barrier seems to be caused by high salt concentration under experimental conditions (i.e. 30% $CaCl_2$). This behaviour is also corroborated experimentally since the poor signal separation of **NP** and **NS** forms were observed in pure D_2O solution even at temperatures close to 273 K.

Selection of right interconversion pathway between the **NP** and **NS** state is not critical for drawn conclusions as the calculated free energy is a state function and thus the calculated difference between **NS** and **NP** states is path independent (within numerical accuracy). In the case of the guest **11**, we have shown that interconversion can take place by threading the guest through β-CD cavity. However, this does not exclude other possibilities including partial or full complex dissociation, which can be preferred by other guests (**5a**, **5b**, **10**, and **12**) showing different bulkiness of the cationic part. Experimentally, the interconversion by the full complex dissociation is not excluded even for **11** as the combination of ITC binding affinity (ΔG_b=−34.2 kJ·mol^{-1}) and kinetic data (ΔG_a=66.2 kJ·mol^{-1}) from NMR measurements indicates that the transition state for interconversion is above the dissociated state.

Linking calculated structures with NMR data

^{1}H NMR experiments and molecular modelling suggested that there are two stable arrangements of the complex. Whereas the adamantane cage occupies the interior of β-CD cavity in both complexes, the phenyltrimethylammonium moiety is protruding either from the primary (P) or secondary (S) cyclodextrin portal (Figure 5). We performed a 2D NOE experiment[25] on the sample related to line iv in Figure 3 to assign the NMR signal subsets to the corresponding supramolecular arrangements.

We found a different pattern of dipolar ^{1}H–^{1}H contacts between **NP** and **NS** binding modes (Figure 6). While contacts between phenyl ring and β-CD were detected for **NP** (H5'···H_d, and H5'···H_e), analogous contacts with H5' or H3' were not observed for **NS**. This qualitatively agrees with the interior arrangement of **11** inside the β-CD cavity. In both orientations, the adamantane cage prefers a position of about 1.0 Å off a plane going through β-CD glycosidic bridges towards the secondary rim (Figure S62). Such asymmetry moves the phenyl ring closer to interior protons of β-CD in **NP**, but farther in **NS**.

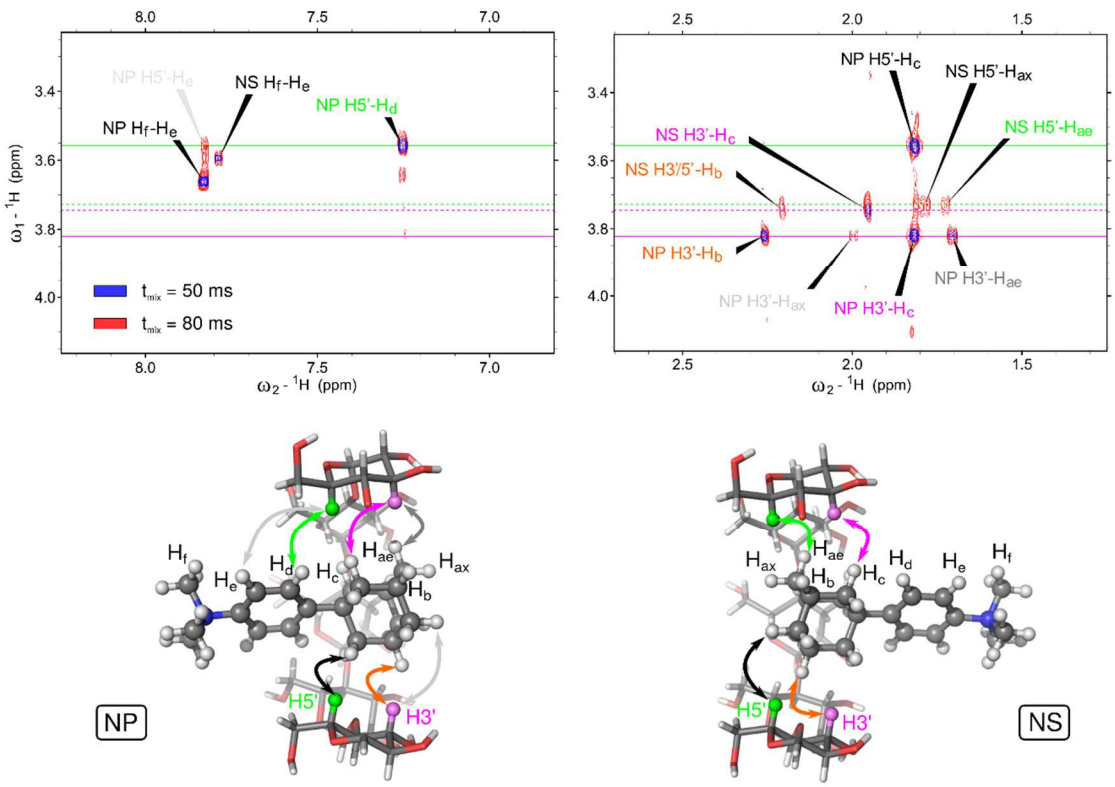

Figure 6 Portions of the 2D NOE spectrum (*top*) recorded on a 1:1 mixture of guest **11** and β-CD in 30% $CaCl_2$ in D_2O at 273 K at two mixing times. Shorter mixing time (50 ms) provided information about close H–H contacts (up to 3 Å), whereas a longer mixing time (80 ms) provided information about longer H–H contacts (up to 6 Å). Horizontal lines represent H5' and H3' signals for **NP** (solid) and **NS** (dashed) forms. Idealised geometries of **NP** and **NS** forms with annotations of hydrogen atoms and contacts (*bottom*). Corresponding intermolecular dipolar contacts in the NOESY spectrum and idealised structures are coded by matching colours.

For the full assignment of NOESY data, we calculated proton contacts from unbiased molecular dynamics simulations of **NP** and **NS** states (Figure 7). Most of the close contacts, which exhibited a higher occurrence for shorter distances, were also observed in the NOESY spectrum. However, we found a few exceptions. H3'···H_{ax} shows small occurrence for both forms and only **NP** H3'···H_{ax} was detected in NOESY at a longer mixing time. Next, NOESY did not detect any contact of H3' with either aromatic protons H_d and H_e, although RDF showed high occurrences for **NS** H3'···H_d. We assume that the sidearm of the guest containing the phenyl ring, which is outside of β-CD, is wiggling fast, especially in the **NS** state, resulting in an NOE peak broadening and its disappearance from the NMR spectrum. This behaviour is also supported by the free energy surface, which shows a larger basin prolonged in α_{PVANG} dimension for **NS** compared to **NP**.

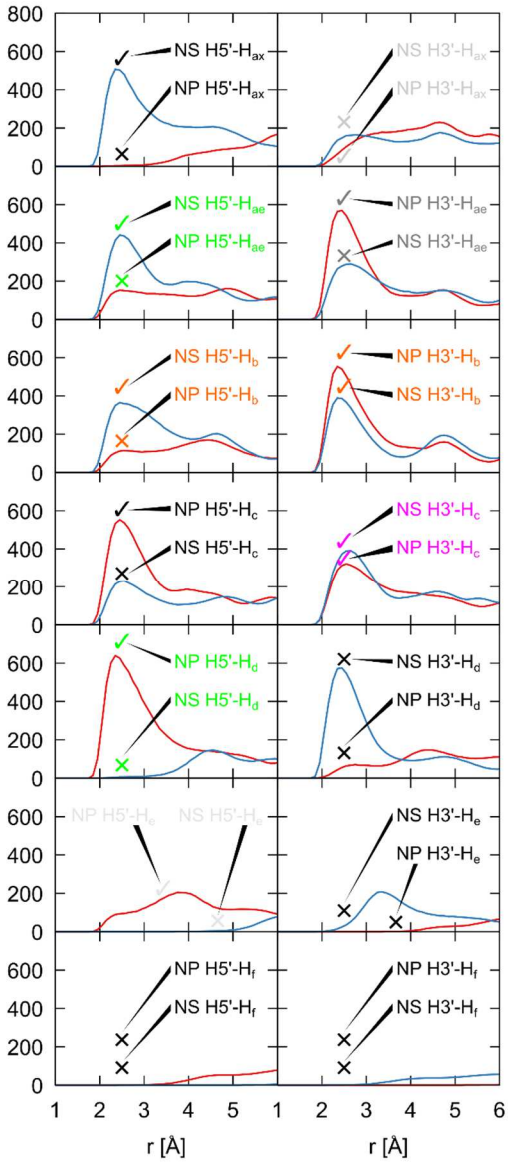

Figure 7 Radial distribution occurrence for contacts between proton of guest **11** and the H5'(*left*) and H3'(*right*) protons of β-CD from unbiased molecular dynamics of **NP** and **NS** orientations. Detected (✓) and undetected (×) dipolar contacts in the NOESY spectrum are colour coded in the same way as in Figure 6.

In addition to 2D NOE experiments, we analysed trends in complexation-induced NMR shifts. NMR data indicate that H5' of β-CD in the **NP** form is more shielded compared to **NS** ($\Delta\delta_{\mathrm{H5'}}^{\mathrm{NP-NS}}$=−0.18 ppm), which can be attributed to the ring-current through-space effects of the phenyl ring being closer to H5' in structure. An opposite but smaller difference in the NMR chemical shift was also observed for the H3' signal ($\Delta\delta_{\mathrm{H3'}}^{\mathrm{NP-NS}}$=+0.08 ppm). For comparison, we calculated the through-space shielding (as nucleus-independent chemical shifts [NICS]) on a regular grid around the benzene molecule. These data were superimposed on the phenyl ring in each snapshot of unbiased molecular simulations of **NP** and **NS** states to obtain an average effect on the host protons.[10] Obtained data $\Delta\delta_{\mathrm{H5'}}^{\mathrm{NP-NS}}$=−0.17 ppm and $\Delta\delta_{\mathrm{H3'}}^{\mathrm{NP-NS}}$ =+0.19 ppm shows good qualitative agreement with experimental data confirming that structures observed in molecular simulations are similar to those observed experimentally.

We have also compared ^{1}H NMR chemical shifts of ligand atoms between the binding modes. The largest relative perturbation was observed for the terminal H_{ax} atoms, which are located on one side of β-CD, and the H_c and H_d protons, which are located on the opposite side of β-CD, with chemical shift changes of $\Delta\delta_{H_{ax}}^{NP-NS}$=+0.21 ppm, $\Delta\delta_{H_c}^{NP-NS}$=–0.12 ppm and $\Delta\delta_{H_d}^{NP-NS}$=–0.33 ppm, respectively. We assume that the changes are induced mainly by desolvation of hydrogen atoms upon encapsulation and the shielding effect of the cavity interior of β-CD. Therefore, the effect of desolvation was evaluated in the next step. The radial distribution function for ligand···water calculated from MD simulations (Figure S63) clearly shows that H_{ax} is substantially more accessible to solvent molecules in the **NP** orientation, whereas the H_c and H_d atoms are exposed more in the **NS** orientation.

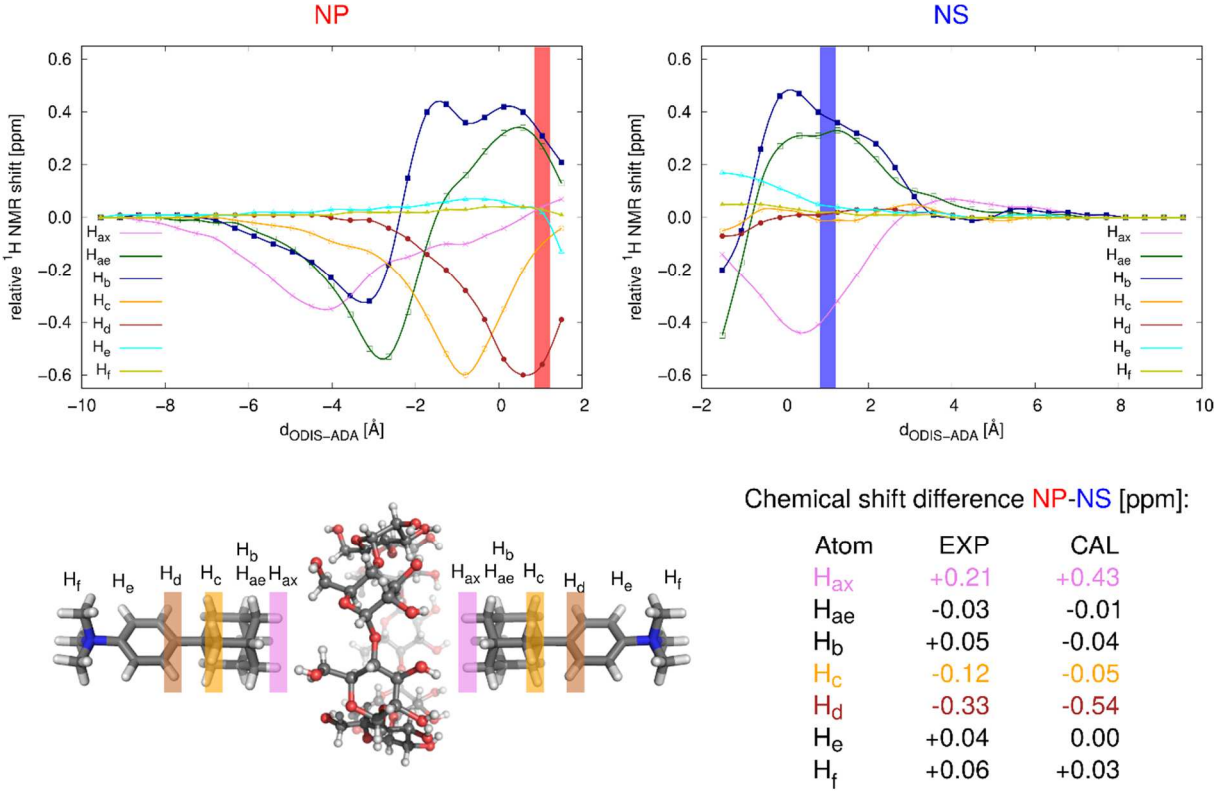

Chemical shift difference NP-NS [ppm]:

Atom	EXP	CAL
H_{ax}	+0.21	+0.43
H_{ae}	-0.03	-0.01
H_b	+0.05	-0.04
H_c	-0.12	-0.05
H_d	-0.33	-0.54
H_e	+0.04	0.00
H_f	+0.06	+0.03

Figure 8 Rigid body scan shows changes of ^{1}H relative chemical shift of the ligand **11** upon encapsulation into the β-CD cavity through primary (*left*) and secondary (*right*) portal calculated by the DFT approach in an implicit water solvent. Resulting experimental differences in NMR chemical shifts between **NP** and **NS** orientation $\Delta\delta^{NP-NS}$ are summarised in the table insert. Data shown in the CAL column refer to differences in NMR shifts predicted by the DFT for mutual geometries (red and blue stripes in the graphs) corresponding to unbiased molecular dynamics for **NP** and **NS** (Figure S62).

To capture both desolvation and the shielding effect, we attempted to calculate NMR shifts of ligand H-atoms as a function of ligand orientation (**NP**/**NS**) and axial distance between the ligand and centre of mass of β-CD. The NMR shielding was calculated by employing the DFT approach in an implicit water model applied on a series of structures differing just in ligand···host separation (for details, see Supporting Information). An obtained scan depicted in Figure 8 corroborates that H_{ax} in the **NS** shows lower chemical shifts compared to the **NP** orientation. Furthermore, H_d and H_c exhibit significantly lower chemical shifts in the **NP** since they are exposed to the narrower primary portal. Despite the limitation of the employed model, which does not account for geometry relaxation or tilting of the guest upon complexation, the analysis provided good agreement between experimental and calculated changes of chemical shifts of **NP** and **NS** forms (see the table insert in Figure 8).

Conclusions

In concert with our original motivation, which was focused on the preparation of suitable binding motifs for CB7 with moderate affinity, we synthesised five new model guests and determined their binding properties towards CB7 and β-CD. The guests consist of 1-adamantylphenyl scaffold and various cationic moiety, namely ammonium (**11**), imidazolium (**5a**, **5b**, **10**) and pyridinium (**12**). We prepared only methylated guests (with exception to pyridinium salt **12**), but the employed procedure is general and its extension to other alkylating agents is feasible. Particularly imidazolium derivatives can serve for the construction of advanced supramolecular components such as multitopic guests.[26]

Combining data from ITC and NMR, we found that all examined guests bind CB7 with an adamantane cage positioned inside the CB7 cavity. The values of association constants K_{CB7} were determined within the range (0.6–5)×10^{10} M^{-1}. These values match our expectations because they lie nearly in the middle of the interval given by association constants of previously reported guests[10] of similar structure: 4-(1-adamantylcarbonyl)phenylmethyl(methyl)imidazolium iodide (K_{CB7}=2.6×10^{8} M^{-1}) and 1-adamantylmethyl(methyl)imidazolium iodide (K_{CB7}=3.7×10^{12} M^{-1}). For them, we demonstrated that ion–dipole interactions contribute to the stabilisation of the complex with CB7 as very little for the former and significantly for the latter. In this work, we confirmed this trend. All of the guests with the phenyl spacer displayed intermediate values of association constants towards CB7 (K≈10^{10} M^{-1}). In other words, the stability of the complex negatively correlates with the length of the linker between the adamantane cage and the cationic moiety as the contribution of the ion-dipole interactions decreases with the length of the linker.

According to the ITC experiments, our new guests showed surprisingly high association constants with β-CD within the range of (0.6–2.6)×10^{6} M^{-1}. The highest value ($K_{β\text{-}CD}$=2.6×10^{6} M^{-1}), which was obtained for guest **5a**, rivals the highest binding constant ever reported for a 1:1 β-CD complex (triamantane-9-carboxylic acid, $K_{β\text{-}CD}$=2.9×10^{6} M^{-1}).[3] We suggest our ligand **5a** as a reasonable choice for the design of multitopic guests because the overall yield of the corresponding building block **4a** from commercially available 1-bromoadamantane was 30% whereas the yield of triamantane-9-carboxylic acid was 19% from a rather uncommon triamantane.[27] ^{1}H NMR experiments on complexes of β-CD with our guests revealed a moderate-exchange process in the mixtures containing an excess of β-CD in water. We assumed that two distinct geometrical forms of the guest@β-CD complex were present in equilibrium. This hypothesis was strongly supported by ^{1}H NMR experiments on the mixture of guest **11** and β-CD. We performed these measurements in 30% $CaCl_2$ solution in D_2O to be able to record spectra within the temperature range of 258–303 K. We observed two unambiguously resolved subsets of signals for the guest below 273 K. The dipolar contacts observed in 2D NOE experiments allowed us to identify two geometrical arrangements where phenyltrimethylammonium moiety protrudes either from the primary (**NP**) or secondary (**NS**) portal of β-CD. According to ^{1}H NMR spectrum, the **NP**:**NS** ratio was 60:40 in 30% $CaCl_2$ at 273 K. Finally, two different binding modes of guest **11** inside the β-CD cavity were confirmed by the unbiased and biased MD simulations. Calculated free energy shows that the **NP** and **NS** arrangements are of comparable free energies. We also described two pathways for their interconversion, which both took place through partial complex dissociation. The rate-determining step had barrier 41 kJ·mol^{-1} under simulation conditions (NaCl solution), which is close to the experimentally determined value of 68 kJ·mol^{-1} ($CaCl_2$ solution).

In this work, we presented convenient synthetic approaches leading to new guests, which are suitable for binding into β-CD and CB7 macrocycles with tuneable affinity. The structural characterisation of such supramolecular complexes, which is essential for further rational design, is challenging due to its inability to get single-crystals suitable for the X-ray diffraction analysis. Therefore, we combined low-temperature NMR in salt water and computer simulations to obtain

comprehensive information about their structure. We demonstrated that this state-of-the-art methodology is able to throw light on intrinsic structure of cyclodextrin complexes. Despite the long history of the cyclodextrin chemistry, actual orientation of the guests in the conical CD cavity has not been studied thoroughly, most likely due to fast equilibration of relatively weak complexes. As the particular forms can differ in their binding strengths, detailed knowledge of the complex geometry is especially important if only one rim of the cyclodextrin macrocycle can be employed for host–guest interactions in considered systems. We believe that our methodology is suitable for the study of functional supramolecules, which can act as drug delivery systems, molecular sensors or switches.

Experimental

General information

All solvents, reagents and starting compounds were of analytical grade, purchased from commercial sources and used without further purification, if not stated otherwise. Tolyladamantanes **2a** and **2b**,[28] bromoderivatives **3a** and **3b**,[29] 1-phenyladamantane (**6**),[30] nitro derivative **7**[31] and aniline **8**[32] were prepared following previously published procedures. Protocols are given in detail in Supporting Information. Melting points were measured on a Kofler block and are uncorrected. Elemental analyses (C, H and N) were performed using a Thermo Fisher Scientific Flash EA 1112. HRMS analyses were performed on an Agilent 6230 Time-of-Flight spectrometer with an electrospray ion source. NMR spectra were recorded using a Bruker Avance NEO 500 MHz spectrometer operating at frequencies of 500.21 MHz (^{1}H) and 125.78 MHz (^{13}C), a Bruker Avance III HD 700 MHz spectrometer operating at a frequency of 700.80 MHz (^{1}H), a Bruker Avance III HD 950 MHz spectrometer operating at a frequency of 950.33 MHz (^{1}H) and a Jeol JNM-ECZ400R/S3 spectrometer operating at frequencies of 399.78 MHz (^{1}H) and 100.53 MHz (^{13}C). ^{1}H- and ^{13}C-NMR chemical shifts were reported as parts per million (ppm) and referenced to the signal of the solvent (^{1}H: δ[residual DMSO-d_5]=2.50 ppm, δ[residual HDO]=4.70 ppm, δ[residual $CHCl_3$]=7.27 ppm; ^{13}C: δ[DMSO-d_6]=39.52 ppm, δ[$CDCl_3$]=77.16 ppm). The mixing time for 2D ^{1}H-^{1}H NOESY experiment[25,33] was adjusted to 50 or 80 ms. Signal multiplicity is indicated by ‘s’ for singlet, ‘d’ for doublet, ‘m’ for multiplet and ‘um’ for unresolved multiplet. IR spectra were recorded using a Smart OMNI-Transmission Nicolet iS10 spectrophotometer. Samples were measured in KBr pellets. Electrospray mass spectra (ESI–MS) were recorded using an amaZon X ion-trap mass spectrometer (Bruker Daltonics, Bremen, Germany) equipped with an electrospray ionisation source. All the experiments were conducted in the positive-ion polarity mode. The instrumental conditions used to measure the single imidazolium salts and their mixtures with the host molecules were different; therefore, they are described separately. *Single guests*: Individual samples (with concentrations of 0.5 μg·cm^{-3}) were infused into the ESI source in MeOH:H_2O (1:1, v:v) solutions using a syringe pump with a constant flow rate of 3 μl·min^{-1}. The other instrumental conditions were as follows: an electrospray voltage of −4.2 kV, a capillary exit voltage of 140 V, a drying gas temperature of 220 °C, a drying gas flow rate of 6.0 dm^3·min^{-1} and a nebuliser pressure of 55.16 kPa. *Host–guest complexes*: An aqueous solution of the guest (12.5 μM) and the equimolar amount of the corresponding host (in the case of **12**@β-CD 3.0 eq of host were used) was infused into the ESI source at a constant flow rate of 3 μl·min^{-1}. The other instrumental conditions were as follows: an electrospray voltage of −4.0 kV, a capillary exit voltage of 140 V up to −50 V, a drying gas temperature of 300 °C, a drying gas flow rate of 6.0 dm^3·min^{-1}, and a nebuliser pressure of 206.84 kPa. Nitrogen was used as both the nebulising and drying gas for all of the experiments. Tandem mass spectra were collected using CID with He as the collision gas after the isolation of the required ions. Isothermal titration calorimetry measurements were carried out in H_2O using a VP–ITC MicroCal instrument at 303 K. The concentrations of the host in the cell and the guest in the microsyringe were approximately 0.05 mM

and 0.50 mM for CB7 and 0.15 mM and 1.50 mM for β-CD, respectively. The raw experimental data were analysed with the MicroCal ORIGIN software. The heats of dilution were taken into account for each guest compound. The data were fitted to a theoretical titration curve using the One Set of Sites model. If needed, a competitive approach[7] was employed using a 1-methyl-3-hexylimidazolium chloride (K_{CB7}=1.23×10^7 dm^3·mol^{-1}) as a competitor. The *K* values obtained from the competitive titrations were verified using two different concentrations of a competitor. All titrations were performed in triplicate.

X-ray Crystallographic Analysis of 3b and 4b

The crystals of **3b** were grown in the mixture of **3b**/**3a** after column chromatography at room temperature. The single crystals were collected by tweezers and washed using EtOAc. Identical crystal structure has been very recently reported.[34] The crystals of **5b** were grown by slow evaporation of D_2O at room temperature. Single-crystal X-ray diffraction data were collected on a Rigaku MicroMax-007 HF rotating anode four-circle diffractometer using Mo Kα radiation at 120 K. The non-hydrogen atoms were refined anisotropically, hydrogen atoms were refined as riding on their carrier atoms. CrystalClear and CrysAlisPro software packages were used for data collection and reduction.[35] The structures were solved by the direct methods procedure and refined by full matrix least-squares methods on F^2 using SHELXT and SHELXL.[36] The crystallographic data of **3b** and **5b** were deposited in the Cambridge Crystallographic Data Centre with the deposition numbers CCDC 1956556 and CCDC 1956557, respectively. For further details of XRD measurement see the Supporting Information.

Computational methods

Two complexes of **11**@β-CD were built by placing **11** into the cavity of β-CD in two possible arrangements **NP** and **NS**. Each complex was separately immersed into a truncated octahedral box filled with TIP3P water and sodium and chloride ions (c_{NaCl}≈0.14 M). General Amber Force Field 2[37] was utilised for **11**, whereas β-CD was described by GLYCAM06.[38] Unbiased MD simulations were performed in the Amber 16.0 package[39] at 300 K and 100 kPa and were 1 μs long each. The interconversion between **NP** and **NS** was further studied by biased MD using the ABF method[40] enhanced by the MWA approach[41] in the modified pmemd program from the Amber package coupled with PMFLib.[42] The total length of the biased ABF/MWA sampling was 4.4 μs. The resulting free energy surface was reconstructed from the calculated mean forces by the Gaussian Process Regression (GPR)[43] with optimised GPR hyperparameters. All errors are reported at three standard deviations.

Snapshots from the unbiased MD were also used to investigate how shielding of the benzene ring found in **11** propagates onto the protons of β-CD via the NICS approach.[10] Changes in chemical shifts were calculated at B3LYP/def2-SVP(β-CD), def2-TZVPP(ligand)/SMD level of theory. An extended description of the computational methodology is provided in Supporting Information.

Synthesis

1-Tolyladamantanes 2a and 2b

Method A: The reaction was carried out according to a slightly modified published procedure.[28] The catalyst $InCl_3·H_2O$ (0.0196 g, 0.082 mmol) was dried prior to the reaction by refluxing with $SOCl_2$ (5 cm^3) which was then evaporated. To a dry catalyst, compound **1** (0.3611 g, 1.68 mmol) and dry toluene (5 cm^3) were added. The reaction mixture was stirred under an inert atmosphere at 30 °C (maintained using an oil bath) until GC–MS indicated consumption of the compound **1**. The reaction was quenched with 115 cm^3 of 10% $NaHCO_3$ and mixture was extracted with AcOEt (3 × 10 cm^3). Combined organic portions were washed with brine (15 cm^3) and dried over anhydrous sodium sulphate. Solvents were evaporated under reduced pressure and the crude product was purified by column chromatography

(silica gel, petroleum ether) to isolate a mixture of **2a** and **2b** as a colourless microcrystalline powder (0.3529 g, 1.56 mmol, yield 93 %, **2a**:**2b** = 19:1 according to GC–MS).
Method B: Compound **1** (2.0463 g, 9.51 mmol) was added to a dispersion of $AlCl_3$ (0.0450 g, 0.34 mmol) in dry toluene (25 cm^3). The reaction mixture was stirred under an inert atmosphere at −3 °C (cooled by ice/water/NaCl mixture) and monitored using GC–MS. Since the compound **1** was completely consumed, the reaction was quenched with 10% $NaHCO_3$ solution (15 cm^3) and extracted with AcOEt (3 × 10 cm^3). Combined organic portions were washed with brine (15 cm^3), dried over sodium sulphate and the solvents were evaporated under reduced pressure to obtain a yellowish powder. The crude product was purified by column chromatography (silica gel, petroleum ether) to isolate a mixture of **2a** and **2b** as a colourless microcrystalline powder (1.1560 g, 5.11 mmol, yield 54 %, **2a**:**2b** = 1:2 according to GC–MS). MS (EI, 70 eV): **2a** 41 (12); 65 (7); 77 (11); 79 (13); 91 (20); 94 (13); 105 (21); 115 (13); 133 (7); 141 (7); 153 (5); 154 (10); 155 (6); 169 (100); 170 (19); 183 (12); 226 (73); 227 (14) m/z (%); **2b** 41 (14); 65 (7); 67 (5); 77 (13); 79 (17); 91 (22); 940 (27); 105 (21); 115 (13); 117 (6); 128 (11); 132 (15); 141 (9); 153 (5); 154 (10); 155 (7); 169 (100); 170 (21); 183 (14); 226 (77); 227 (15) m/z (%).

1-(Bromomethylphenyl)adamantanes 3a and 3b were prepared following the previously described procedure.[29] Typically, *N*-bromosuccinimide (0.2514 g, 1.41 mmol) was added to a solution of **2a** and **2b** mixture (0.3070 g, 1.36 mmol, **2a**:**2b** = 19:1) in dry CCl_4 (5 cm^3). The reaction mixture was refluxed under an inert atmosphere using an oil bath and irradiated by 60 W tungsten lamp for 1 h. After cooling to room temperature, succinimide was filtered off on a sintered-glass funnel and solvent was evaporated under reduced pressure to obtain a yellow oil. The crude product was purified by column chromatography (silica gel, petroleum ether) to isolate a mixture of **3a** and **3b** as a yellowish powder (0.2961 g, 0.97 mmol, yield 71 %, **3a**:**3b** = 19:1 according to GC–MS). The same procedure was repeated with the 1:2 mixture of **2a**:**2b** to yield oily product from which **2b** slowly crystallised at room temperature. MS (EI, 70 eV): **3a** 41 (6), 77 (5), 79 (6), 91 (13), 104 (5), 105 (9), 115 (8), 131 (11), 167 (6), 168 (6), 169 (10), 225 (100), 226 (24), 304 (2), 306 (2) m/z (%); **3b** 77 (7), 79 (12), 91 (15), 93 (5), 94 (5), 128 (8), 129 (6), 141 (6), 167 (10), 169 (13), 225 (100), 226 (27), 304 (4), 306 (4) m/z (%).

1-Phenyladamantane (6) was prepared following the previously described procedure.[30] Compound **1** (0.2093 g, 0.97 mmol) was added to a dispersion of $AlCl_3$ (0.0293 g, 0.22 mmol) in dry benzene (10 cm^3). The reaction mixture was stirred under an inert atmosphere at room temperature and the reaction progress was monitored using GC–MS. When GC indicated the complete consumption of the compound **1**, the reaction was quenched with 10% $NaHCO_3$ solution (10 cm^3) and extracted with AcOEt (3 × 10 cm^3). Combined organic portions were washed with brine (15 cm^3), dried over sodium sulphate and the solvents were evaporated under reduced pressure to obtain a colourless powder. The crude product was purified by column chromatography (silica gel, petroleum ether) to obtain a colourless microcrystalline powder (0.1792 g, 0.84 mmol, yield 87 %). M. p.: 89–90 °C, lit. m. p.: 87–89 °C.[44] ^1H and ^{13}C NMR data correspond to that previously published.[45]

1-(4-Nitrophenyl)adamantane (7) was prepared following the previously described procedure.[31] Starting acetyl nitrate was prepared from Ac_2O (23 cm^3) and a mixture of conc. HNO_3 (9.3 cm^3) and conc. H_2SO_4 (0.45 cm^3) in a double-coated reaction flask at −15 °C. Subsequently, a dispersion of **6** (2.005 g, 9.44 mmol) in acetic anhydride (40 cm^3) was slowly added dropwise while the internal temperature of the reaction mixture was maintained within the range of −15 to −5 °C. When the compound **6** was consumed (according to TLC or GC), the reaction was quenched by addition of crushed ice to precipitate a pale yellow solid. Water dispersion was extracted with several portions of Et_2O, collected organic portions were treated with water (2 × 50 cm^3), saturated $NaHCO_3$ solution and dried over sodium sulphate. The solvent was evaporated and the crude product was crystallised from

MeOH to obtain yellowish needles (1.3851 g, 5.38 mmol, yield 57%). M. p.: 128–130 °C, lit. m. p.: 129–130 °C.[46] ^{1}H NMR ($CDCl_3$, 500 MHz): δ8.17 (d, 2H, *J*=8.4 Hz), 7.51 (d, 2H, *J*=8.4 Hz), 2.15 (m, 3H), 1.94 (m, 6H), 1.76–1.85 (m, 6H).

4-(1-Adamantyl)aniline (8) was prepared following a slightly modified procedure reported previously.[32] Compound **7** (3.2153 g, 12.50 mmol) was dissolved in MeOH (250 cm^3) and conc. HCl (36 cm^3) was added. Portions of iron powder (approx. 1.65 g, 30 mmol) were added successively into the refluxed (using an oil bath) and stirred mixture unless TLC indicated the consumption of **7**. The pH of the reaction mixture was controlled and kept acidic by addition of small portions of conc. HCl. After five portions of iron were added, the mixture was poured to 15% NaOH solution (150 cm^3) and extracted several times with Et_2O. Collected organic portions were washed with brine, dried over sodium sulphate and concentrated under reduced pressure to obtain brown solid (2.1813 g, 9.60 mmol, yield 77 %). This crude material was used in further steps without purification. M. p.: 90–92 °C, literature m. p.: 98–101 °C.[47] ^{1}H NMR (DMSO-d_6, 400 MHz): δ6.98 (m, 2H), 6.49 (m, 2H), 4.75 (s, 2H), 2.02 (um, 3H), 1.77 (m, 6H), 1.70 (um, 6H). $^{13}C\{^1H\}$ NMR (DMSO-d_6, 101 MHz): δ146.0, 138.4, 124.8, 113.7, 43.0, 36.3, 34.7, 28.4. MS (EI, 70 eV): 227 (70), 170 (100), 152 (3), 133 (30), 115 (5), 91 (12), 77(9) m/z (%).

1-(4-(1-Adamantyl)benzyl)-1*H*-imidazole (**4a**) was prepared following the previously described procedure.[10,21] The commercial NaH (60%, 0.0597 g, 1.49 mmol) was washed with dry pentane under an inert atmosphere to remove mineral oil. After preparing a dispersion of NaH in DMF (3 cm^3), a solution of imidazole (0.1006 g, 1.48 mmol) in DMF (5 cm^3) was slowly added. This reaction mixture was stirred for 15 minutes and the solution of bromides **3a** and **3b** (0.2981 g, 0.98 mmol, **3a**:**3b** = 19:1) in DMF (3 cm^3) was added in one portion. The reaction mixture was heated at 120–130 °C using an oil bath and stirred until GC–MS indicated the complete consumption of starting alkylbromides. After four hours, the reaction mixture was poured into crushed ice and extracted with CH_2Cl_2 (5 × 20 cm^3). Combined organic portions were washed with brine (20 cm^3) and dried over sodium sulphate. After the removal of the solvent under reduced pressure, the crude product was purified by repeated column chromatography (silica gel, $CHCl_3$:AcOEt, 1:1, v:v). After two runs on the column, a colourless microcrystalline powder of **4a** was obtained (0.1367 g, 0.47 mmol, yield 48%). M.p.: 152–154 °C. Anal. Calcd for $C_{20}H_{24}N_2$: C, 82.15; H, 8.27; N, 9.58. Found: C, 82.03; H, 8.33; N, 9.41. ^{1}H NMR ($CDCl_3$, 500 MHz): δ8.22 (s, 1H), 7.37 (m, 2H), 7.17 (um, 2H), 6.98 (s, 1H), 5.21 (s, 2H), 2.10 (um, 3H), 1.89 (m, 6H), 1.77 (m, 6H). $^{13}C\{^1H\}$ NMR ($CDCl_3$, 126 MHz): δ152.3, 136.4, 131.6, 127.7, 125.9, 125.8, 119.8, 51.6, 43.1, 36.7, 36.2, 28.9. IR (KBr): 3448 (w), 3105 (sh), 3098 (vw), 3052 (vw), 3023 (vw), 2965 (sh), 2920 (sh), 2905 (vs), 2848 (s), 1507 (w), 1448 (w), 1417 (vw), 1344 (vw), 1320 (vw), 1285 (vw), 1280 (sh), 1262 (vw), 1249 (sh), 1237 (sh), 1231 (m), 1231 (m), 1126 (vw), 1112 (sh), 1108 (vw), 1102 (vw), 1080 (w), 1070 (w), 1032 (w), 1016 (w), 976 (vw), 907 (m), 841 (sh), 836 (vw), 811 (w), 800 (m), 758 (w), 735 (m), 710 (sh), 705 (vw), 661 (m), 635(vw),628 (sh), 626 (sh), 598 (vw), 533 (m) cm^{-1}. ESI–MS (pos.) *m/z* (%): 293.2 $[M+H^+]^+$ (100), 585.4 $[2\cdot M+H^+]^+$ (16).

1-(3-(1-Adamantyl)benzyl)-1*H*-imidazole (4b) was prepared following an analogous procedure as described for **4a**. However, the starting mixture of bromides **3a** and **3b** was prepared by Method B. This mixture of **3a** and **3b** (0.4165 g, 1.36 mmol, **3a**:**3b**=1:2) provided a colourless microcrystalline powder of **4b** (0.080 g, 0.27 mmol, yield 20%). M.p.: 136–139 °C. Anal. Calcd for $C_{20}H_{24}N_2$: C, 82.15; H, 8.27; N, 9.58. Found: C, 81.93; H, 8.35; N, 9.48. ^{1}H NMR ($CDCl_3$, 500 MHz): δ7.78 (s, 1H), 7.34 (um, 1H), 7.30 (m, 1H), 7.17 (s, 1H), 7.12 (s, 1H), 6.97 (um, 1H), 6.93 (s, 1H), 5.15 (s, 2H), 2.09 (um, 3H), 1.87 (m, 6H), 1.76 (m, 6H). $^{13}C\{^1H\}$ NMR ($CDCl_3$, 126 MHz): δ152.6, 137.3, 135.4, 129.0, 128.4, 125.3, 124.8, 124.2, 119.7, 51.7, 43.2, 36.8, 36.4, 29.0. IR (KBr): 3100 (vw), 3024 (vw), 2902 (vs), 2846 (vs), 1606 (w),

1587 (vw), 1504 (m), 1449 (w), 1392 (vw), 1367 (vw), 1355 (vw), 1343 (w), 1318 (w), 1278 (w), 1261 (vw),1225 (w), 1184 (vw), 1169 (vw), 1106 (m), 1090 (m), 1073 (m), 1049 (w), 1027 (m), 975 (w), 905 (w), 865 (vw), 815 (vw), 806 (w), 761 (w), 736 (s), 699 (m), 663 (m), 628 (w), 634 (sh), 547 (vw), 442 (vw) cm^{-1}. ESI–MS (pos.) *m/z* (%): 293.2 $[M+H^+]^+$ (100), 585.4 $[2\cdot M+H^+]^+$ (13).

1-(4-(1-Adamantyl)phenyl)-1*H*-imidazole (9) was prepared using a modified literature procedure.[48] A brown dispersion of **8** (0.9955 g, 4.40 mmol), MeOH (32 cm^3) and 40% glyoxal solution (185 µL, 1.62 mmol) was stirred for 19 hours at room temperature. Then, NH_4Cl (0.4705 g, 8.80 mmol) and a 37% HCHO solution (0.704 mL, 8.87 mmol) were added and the reaction mixture was refluxed for one hour using an oil bath. After the reaction mixture cooled down to room temperature, conc. H_3PO_4 (0.616 cm^3, 85%) was slowly added and then the mixture was refluxed for 19 hours. The solvent was evaporated, the remaining oil was poured on an ice-water mixture and pH was adjusted with 40% KOH solution to **10**. This mixture was extracted with AcOEt (5 × 30 cm^3), combined organic phases were washed with brine and the solution was dried with Na_2SO_4 before evaporating the solvent under the reduced pressure. The afforded mixture was purified by column chromatography (silica gel, AcOEt:MeOH, 8:1, v:v) and obtained a crude product (R_f=0.47) that was purified by column chromatography (silica gel, AcOEt) to yield of a brown powder (0.1913 g, 0.69 mmol, yield 42%). M.p.: 116–118 °C. Anal. Calcd for $C_{19}H_{22}N_2$: C, 81.97; H, 7.97; N, 10.06. Found: C, 81.72; H, 8.12; N, 9.93. ^{1}H NMR ($CDCl_3$, 500 MHz): δ8.27 (s, 1H), 7.50 (m, 2H), 7.38 (m, 2H), 7.32 (s, 1H), 7.31 (s, 1H), 2.13 (um, 3H), 1.93 (m, 6H), 1.79 (m, 6H). $^{13}C\{^1H\}$ NMR ($CDCl_3$, 126 MHz): δ 152.2, 135.0, 134.2, 127.4, 126.8, 121.7, 119.1, 43.3, 36.8, 36.4, 29.0. IR (KBr): 3122 (w), 3114 (sh), 3059 (vw), 3040 (vw), 2941 (sh), 2928 (s), 2918 (sh), 2910 (vs), 2898 (sh), 2852 (m), 2845 (sh), 1610 (w), 1584 (vw), 1526 (s), 1518 (sh), 1509 (sh), 1490 (m), 1449 (w), 1371 (vw), 1345 (w), 1306 (m), 1266 (vw), 1257 (m), 1255 (sh), 1245 (w), 1110 (w), 1102 (w), 1057 (m), 1034 (w), 964 (w), 904 (w), 847 (w), 827 (w), 806 (m), 734 (w), 726 (w), 721 (w), 658 (sh), 656 (m), 652 (sh), 623 (vw), 552 (w) cm^{-1}. ESI–MS (pos.) *m/z* (%): 279.1 $[M+H^+]^+$ (100), 301.1 $[M+Na^+]^+$ (15), 557.3 $[2\cdot M+H^+]^+$ (23), 579.4 $[2\cdot M+Na^+]^+$ (15).

A general procedure towards imidazolium salts 5a, 5b and 10. Iodomethane (5 eq., 0.95–3.30 mmol) was added into a solution of imidazole **4a**, **4b** or **9** (1 eq., 0.19–0.66 mmol) in dry toluene (5 cm^3) under an inert atmosphere. The reaction mixture was stirred at room temperature and monitored using TLC until the starting imidazole disappeared. Then, dry Et_2O (2 cm^3) was added to precipitate the imidazolium salt. The solid material was washed five times with dry Et_2O using a centrifuge. Dispersion in Et_2O was transferred into a round-bottom flask and solvent was evaporated to obtain pure imidazolium salt, which was dried in a vacuum to constant weight prior to supramolecular studies.

1-(4-(1-Adamantyl)benzyl)-1*H*-imidazolium iodide (5a) was prepared from compound **4a** (0.0839 g, 0.29 mmol) to yield a colourless powder (0.0884 g, 0.20 mmol, yield 69%). M.p.: 162–164 °C. Anal. Calcd for $C_{21}H_{27}IN_2\cdot 0.8\ H_2O$: C, 56.20; H, 6.42; N 6.24. Found: C, 56.25; H, 6.43; N, 6.22. HRMS (ESI/TOF) m/z: M^+ Calcd for $C_{21}H_{27}N_2$ 307.2169; Found 307.2175. ^{1}H NMR ($CDCl_3$, 500 MHz): δ10.37 (s, 1H), 7.40 (s, 4H), 7.29 (s, 1H), 7.21 (s, 1H), 5.49 (s, 2H), 4.09 (s, 3H), 2.09 (um, 3H), 1.88 (m, 6H), 1.76 (m, 6H). $^{13}C\{^1H\}$ NMR ($CDCl_3$, 126 MHz): δ153.3, 138.1, 129.6, 129.1, 126.3, 123.5, 122.0, 53.9, 43.2, 37.4, 36.8, 36.5, 29.0. IR (KBr): 3440 (m), 3166 (vw), 3131 (vw), 3096 (vw), 3081 (w), 2964 (w), 2925 (sh), 2910 (sh), 2903 (sh), 2889 (sh), 2877 (s), 2849 (s), 1567 (m), 1561 (sh), 1554 (sh), 1514 (w), 1507 (s), 1457 (sh), 1450 (w), 1420 (sh), 1416 (w), 1409 (vw), 1361 (w), 1356 (sh), 1348 (w), 1342 (w), 1332 (vw), 1321 (vw), 1319 (sh), 1273 (vw), 1160 (sh), 1144 (w), 1107 (w), 1104 (sh), 1101 (sh), 1034 (vw), 1022 (w), 1018 (sh), 976 (vw), 862 (vw), 852 (w), 813 (m), 804 (m), 774 (w), 768 (w), 762 (sh), 758 (w), 745 (sh), 710 (w), 691 (w), 664 (sh), 657 (w), 623 (m), 614 (w), 593 (vw), 539 (m) cm^{-1}. ESI–MS (pos.) *m/z* (%): 307.1 $[M^+]^+$ (100).

1-(3-(1-Adamantyl)benzyl)-1*H*-imidazolium iodide (5b) was prepared from compound **4b** (0.0556 g, 0.19 mmol) to yield a colourless powder (0.0509 g, 0.12 mmol, yield 63%). M.p.: 171–173 °C. Anal. Calcd for $C_{21}H_{27}IN_2$: C, 58.07; H, 6.27; N, 6.45. Found: C, 57.94; H, 6.36; N, 6.39. ^{1}H NMR (DMSO-d_6, 500 MHz): δ9.20 (s, 1H), 7.81 (um, 1H), 7.70 (um, 1H), 7.48 (um, 1H), 7.38 (um, 1H), 7.35 (m, 1H), 7.20 (um, 1H), 5.39 (s, 2H), 3.86 (s, 3H), 2.07 (um, 3H), 1.86 (m, 6H), 1.74 (m, 6H). ^{13}C{^{1}H} NMR (DMSO-d_6, 126 MHz): δ151.8, 136.5, 134.5, 128.7, 125.4, 125.2, 125.0, 124.0, 122.3, 52.2, 42.5, 36.1, 35.9, 35.8, 28.2. IR (KBr): 3418 (vw), 3142 (vw), 3126 (vw), 3076 (vs), 3052 (sh), 2971 (w), 2923 (vs), 2911 (vs), 2895 (vs), 2848 (vs), 1605 (w), 1567 (m), 1489 (w), 1448 (sh), 1430 (w), 1372 (w), 1364 (sh), 1344 (w), 1319 (w), 1273 (vw), 1245 (vw), 1201 (vw), 1171 (w), 1151 (vs), 1103 (vw), 1094 (vw), 980 (vw), 976 (vw), 832 (w), 823 (w), 816 (m), 798 (w), 768 (vw), 745 (s), 707 (m), 698 (w), 666 (w), 624 (m), 616 (s), 592 (vw), 545 (vw) cm^{-1}. ESI–MS (pos.) *m/z* (%): 307.1 $[M^+]^+$ (100).

1-(4-(1-Adamantyl)phenyl)-1*H*-imidazolium iodide (10) was prepared from compound **9** (0.1829 g, 0.66 mmol) to yield a colourless powder (0.1246 g, 0.30 mmol, yield 45%). M.p.: 194–196 °C. Anal. Calcd for $C_{20}H_{25}IN_2$: C, 57.15; H, 5.99; N, 6.66. Found: C, 57.07; H, 5.93; N; 6.82. ^{1}H NMR ($CDCl_3$, 500 MHz): δ10.52 (s, 1H), 7.54–7.68 (m, 5H), 7.53 (m, 1H), 4.25 (s, 3H), 2.11 (um, 3H), 1.89 (m, 6H), 1.77 (m, 6H). ^{13}C{^{1}H} NMR ($CDCl_3$, 126 MHz): δ154.3, 136.3, 132.0, 127.4, 124.6, 121.9, 120.9, 43.1, 37.7, 36.7, 36.6, 28.9. IR (KBr): 6453 (sh), 3404 (sh), 3148 (w), 3095 (sh), 3072 (m), 3044 (sh), 3005 (sh), 2928 (sh), 2911 (sh), 2900 (vs), 2885 (sh), 2847 (vs), 2679 (vw), 2656 (vw), 1571 (m), 1551 (m), 1516 (sh), 1508 (w), 1499(w), 1412 (vw), 1384 (w), 1369 (vw), 1359 (vw), 1343 (w), 1317 (vw), 1310 (sh), 1272 (vw), 1251 (vw), 1235 (vw), 1220 (w), 1107 (vw), 1103 (vw), 1077 (w), 1069 (sh), 1033 (vw), 1024 (vw), 1017 (vw), 1013 (vw), 978 (vw), 975(sh), 956 (vw), 938 (vw), 850 (vw), 841 (w), 809 (m), 727 (vw), 657 (vw), 641 (vw), 627 (sh), 614 (w), 610 (w), 564 (w), 551 (w) cm^{-1}. ESI–MS (pos.) *m/z* (%): 293.2 $[M^+]^+$ (100).

(4-(1-Adamantyl)phenyl)trimethylammonium iodide (11) was prepared following a modified literature procedure.[5b] A mixture of **8** (0.1030 g, 0.45 mmol), $NaHCO_3$ (0.0840 g, 1.00 mmol), CH_3I (0.205 cm^3, 3.30 mmol) and MeOH (32 cm^3) was refluxed for eight hours using an oil bath. Then, the second portion of MeI (0.205 cm^3, 3.30 mmol) was added and the reaction mixture was refluxed for additional eight hours. The mixture was cooled down, concentrated under reduced pressure and washed with hot acetone (20 cm^3) to obtain a white solid. The solid crude product was washed with several portions of $CHCl_3$ to separate **11** from inorganic salts, and a yellowish powder was obtained after evaporation of the solvent (0.1069 g, 0.26 mmol, yield 59%). M.p.: 186–188 °C. Anal. Calcd for $C_{19}H_{28}IN$: C 57.43, H 7.10, N 3.53 (%). Found C 57.31, H 7.12, N 3.49 (%). ^{1}H NMR (DMSO-d_6, 500 MHz): δ7.89 (d, 2H, *J*=9 Hz), 7.59 (d, 2H, *J*=9 Hz), 3.60 (s, 9H), 2.07 (brs, 3H), 1.88 (um, 6H), 1.75 (um, 6H). ^{13}C{^{1}H} NMR (DMSO-d_6, 126 MHz): δ152.7, 144.8, 126.3, 120.0, 56.4, 42.2, 35.9, 35.8, 28.1. IR (KBr): 3446 (s), 3016 (w), 3005 (sh), 2927 (sh), 2900 (vs), 2887 (sh), 2847 (s), 2818 (sh), 2678 (vw), 2658 (vw), 1634 (w), 1506 (w), 1456 (w), 1343 (vw), 1318 (vw), 1237 (vw), 1186 (sh), 1182 (sh), 1155 (vw), 1127 (sh), 1123 (sh), 1106 (sh), 1102 (sh), 1068 (vw), 1036 (vw), 1011 (w), 974 (vw), 957 (w), 947 (w), 862 (vw), 850 (sh), 845 (w), 827 (vw), 808 (w), 577 (w) cm^{-1}. ESI–MS (pos.) *m/z* (%): 270.1 $[M^+]^+$ (100).

1-(4-(1-Adamantyl)phenyl)pyridinium chloride (**12**) was prepared using a modified literature procedure.[49] Compound **8** (0.2000 g, 0.88 mmol) and *N*-(2,4-dinitrophenyl)pyridinium chloride (0.198 g, 0.97 mmol) were dissolved in EtOH (10 cm^3). The resulting solution was refluxed for 26 hours using an oil bath. Subsequently, the reaction mixture was cooled to room temperature and EtOH was evaporated under reduced pressure. The crude product was crystallised from AcOEt to yield a dark orange powder (0.1813 g, 0.56 mmol, yield 63%). M.p.: 196–200 °C. Anal. Calcd for $C_{21}H_{24}ClN{\cdot}1.2\ H_2O$: C, 72.58; H, 7.66; N, 4.03. Found: C, 72.69; H, 7.81; N, 3.88. HRMS (ESI/TOF) m/z: M^+ Calcd for

$C_{21}H_{24}N$ 290.1909; Found 290.1902. ^{1}H NMR (DMSO-d_6, 400 MHz): δ9.39 (um, 2H), 8.79 (m, 1H), 8.31 (um, 2H), 7.85 (um, 2H), 7.72 (m, 2H), 2.10 (um, 3H), 1.93 (m, 6H), 1.77 (um, 6H). ^{13}C{^{1}H} NMR (DMSO-d_6, 101 MHz): δ154.1, 146.3, 144.8, 140.4, 128.1, 126.6, 124.3, 42.3, 36.1, 35.9, 28.2. IR (KBr): 3423 (w), 2931 (sh), 2904 (m), 2808 (sh), 1625 (vs), 1616 (sh), 1581 (vs), 1564 (vs), 1543 (sh), 1510 (vs), 1476 (w), 1443 (vs), 1413 (w), 1343 (sh), 1335 (vs), 1332 (vs), 1316 (sh), 1335 (vs), 1332 (vs), 1316 (sh), 1241 (vw), 12202 (sh), 1190 (sh), 1175 (vs), 1135 (m), 1102 (w), 1078 (vw), 1033 (w), 1012 (m), 974 (w), 963 (sh), 917 (vw), 887 (vw), 870 (vw), 845 (sh), 835 (m), 802 (w), 781 (w), 741 (vw), 701 (vw), 680 (w), 644 (vw), 568 (sh), 558 (sh), 539 (m), 520 (sh), 428 (vw), 414 (vw) cm^{-1}. ESI–MS (pos.) *m/z* (%): 290.1 $[M^{+}]^{+}$ (100).

Associated Content
Supporting Information

The Supporting Information is available free of charge at https://pubs.acs.org/doi/...

X-ray data for compound **3b** (CIF)
X-ray data for compound **5b** (CIF)
^{1}H, ^{13}C NMR spectra, X-ray data, ITC and MS data, and computational details (PDF)
Structures in the xyz format (ZIP)

Acknowledgements

The authors thank professor Marek Nečas from Masaryk University for X-ray diffraction analyses of compounds **3b** and **5b**. This work has received funding from the Internal Funding Agency of the Tomas Bata University in Zlín (Grant No. IGA/FT/2020/001) and the Czech Science Foundation (Grant. No. 18-05421S). Part of the research was also done within CEITEC 2020 (LQ1601) project with the financial contribution made by the Ministry of Education, Youths and Sports of the Czech Republic (MEYS CR) within special support paid from the National Programme for Sustainability II funds. CIISB, Instruct-CZ Center of Instruct-ERIC EU consortium, funded by MEYS CR infrastructure project LM2018127, is gratefully acknowledged for the financial support of the measurements at the Core Facilities Josef Dadok National NMR Center and X-ray Diffraction and Bio-SAXS. The computational resources were supported by MEYS CR from the Large Infrastructures for Research, Experimental Development and Innovations project 'e-Infrastructure CZ – LM2018140'.

References

(1) (a) Barrow,S. J.; Kasera, S.; Rowland, M. J.; Barrio, J.; Scherman, O. A.: Cucurbituril-Based Molecular Recognition. *Chem. Rev.* **2015**, *115*, 12320–12406. (b) Rekharsky, M. V.; Inoue Y.: Complexation Thermodynamics of Cyclodextrins. *Chem. Rev.* **1998**, *98*, 1875–1918.

(2) Assaf, K. I.; Nau, W. M.: Cucurbiturils: from synthesis to high-affinity binding and catalysis. *Chem. Soc. Rev.* **2015**, *44*, 394–418.

(3) Schibilla, F.; Voskuhl, J.; Fokina, N. A.; Dahl, J. E. P.; Schreiner, P. R.; Ravoo, B. J.: Host–Guest Complexes of Cyclodextrins and Nanodiamonds as a Strong Non-Covalent Binding Motif for Self-Assembled Nanomaterials. *Chem. Eur. J.* **2017**, *23*, 16059–16065.

(4) (a) Moghaddam, S.; Yang, C.; Rekharsky, M.; Ko, Y. H.; Kim, K.; Inoue, Y.; Gilson, M. K.: New Ultrahigh Affinity Host−Guest Complexes of Cucurbit[7]uril with Bicyclo[2.2.2]octane and Adamantane Guests: Thermodynamic Analysis and Evaluation of M2 Affinity Calculations. *J. Am. Chem. Soc.* **2011**, *133*, 3570–3581. (b) Liu, S. M.; Ruspic, C.; Mukhopadhyay, P.; Chakrabarti, S.;

Zavalij, P. Y.; Isaacs, l.: The Cucurbit[n]uril Family: Prime Components for Self-Sorting Systems. *J. Am. Chem. Soc.* **2005**, *127*, 15959–15967.

(5) (a) Cao, L. P.; Šekutor, M.; Zavalij, P. Y.; Mlinarić-Majerski, K.; Glaser, R.; Isaacs, L.: Cucurbit[7]uril·Guest Pair with an Attomolar Dissociation Constant. *Angew. Chem. Int. Ed.* **2014**, *53*, 988–993. (b) Šekutor, M.; Molčanov, K.; Cao, L. P.; Isaacs, L.; Glaser, R.; Mlinarić-Majerski, K.: Design, Synthesis, and X-ray Structural Analyses of Diamantane Diammonium Salts: Guests for Cucurbit[n]uril (CB[n]) Hosts. *Eur. J. Org. Chem.*, **2014**, 2533–2542.

(6) Jelínková, K.; Surmová, H.; Matelová, A.; Prucková, Z.; Rouchal, M.; Dastychová, L.; Nečas, M.; Vícha, R.: Cubane Arrives on the Cucurbituril Scene. *Org. Lett.* **2017**, *19*, 2698–2701.

(7) Rekharsky, M. V.; Mori, T.; Yang, C.; Ko, Y. H.; Selvapalam, N.; Kim, H.; Sobransingh, D.; Kaifer, A. E.; Liu, S.; Isaacs, L.; Chen, W.; Moghaddam, S.; Gilson, M. K.; Kim, K.; Inoue, Y.: A synthetic host–guest system achieves avidin-biotin affinity by overcoming enthalpy–entropy compensation. *Proc. Natl. Acad. Sci. U. S. A.* **2007**, *104*, 20737–20742.

(8) (a) Chyba, J.; Novák, M.; Munzarová, P.; Novotný, J.; Marek, R.: Through-Space Paramagnetic NMR Effects in Host-Guest Complexes: Potential Ruthenium(III) Metallodrugs with Macrocyclic Carriers. *Inorg. Chem.* **2018**, *57*, 8735–8747. (b) Malali, S.; Chyba, J.; Knor, M.; Horní, M.; Nečas, M.; Novotný, J.; Marek, R.: Zwitterionic Ru(III) Complexes: Stability of Metal–Ligand Bond and Host–Guest Binding with Cucurbit[7]uril. *Inorg. Chem.* **2020**, *59*, 10185–10196.

(9) Kolman, V.; Marek, R.; Střelcová, Z.; Kulhánek, P.; Nečas, M.; Švec, J.; Šindelář, V.: Electron Density Shift in Imidazolium Derivatives upon Complexation with Cucurbit[6]uril. *Chem. Eur. J.* **2009**, *15*, 6926–6931.

(10) Branná, P.; Černochová, J.; Rouchal, M.; Kulhánek, P.; Babinský, M.; Marek, R.; Nečas, M.; Kuřitka, I.; Vícha, R.: Cooperative Binding of Cucurbit[n]urils and β-Cyclodextrin to Heteroditopic Imidazolium-Based Guests. *J. Org. Chem.* **2016**, *81*, 9595–9604.

(11) (a) Ding, C.; Liu, Y.; Wang, T.; Fu, J.: Triple-stimuli-responsive nanocontainers assembled by water-soluble pillar[5]arene-based pseudorotaxanes for controlled release. *J. Mater. Chem. B* **2016**, *4*, 2819–2827. (b) Wang, M.-D.; Chen, T.; Ding, C.-D.; Fu, J.-J.: Mechanized silica nanoparticles based on reversible bistable [2]pseudorotaxanes as supramolecular nanovalves for multistage pH-controlled release. *Chem. Commun*. **2014**, *50*, 5068–5071. (c) Sojka, M.; Fojtů, M.; Fialová, J.; Masařík, M.; Nečas, M.; Marek, R.: Locked and Loaded: Ruthenium(II)-Capped Cucurbit[n]uril-Based Rotaxanes with Antimetastatic Properties. *Inorg. Chem.* **2019**, *58*, 10861–10870.

(12) (a) Wang, B.; Han, J.; Bender, M.; Hahn, S.; Seehafer, K.; Bunz,U. H. F.: Poly(para-phenyleneethynylene)-Sensor Arrays Discriminate 22 Different Teas. *ACS Sens.* **2018**, *3*, 504–511. (b) Hu,J.-P.; He, J.-X.; Fang, H.; Yang, H.-H.; Zhang, Q.; Lin, Q.; Yao, H.; Zhang, Y.-M.; Wei, T.-B.; Qu, W.-J.: A novel pillar[5]arene-based emission enhanced supramolecular sensor for dual-channel selective detection and separation of Hg^{2+} *New. J. Chem.* **2020**, *44*, 13157–13162. (c) Liu, Y.-C.; Nau, W. M.; Hennig, A.: A supramolecular five-component relay switch that exposes the mechanistic competition of dissociative versus associative binding to cucurbiturils by ratiometric fluorescence monitoring. *Chem. Commun.* **2019**, *55*, 14123–14126.

(13) Yan, Z.; Huang, Q.; Liang, W.; Yu, X.; Zhou, D.; Wu, W.; Schruma, J. J.; Yang, C.: Enantiodifferentiation in the Photoisomerization of (Z,Z)-1,3-Cyclooctadiene in the Cavity of γ-

Cyclodextrin–Curcubit[6]uril-Wheeled [4]Rotaxanes with an Encapsulated Photosensitizer. *Org. Lett.* **2017**, *19*, 898–901.

(14) Connors, K. A.; Pendergast, D. D.: Microscopic Binding Constants in Cyclodextrin Systems: Complexation of a-Cyclodextrin with Sym-1,4-disubstituted Benzenes. *J. Am. Chem. Soc.* **1984**, *106*, 7607–7614.

(15) (a) Tootoonchi, M. H.; Sharma, G.; Calles, J.; Prabhakar, R.; Kaifer, A. E.: Cooperative Self-Assembly of a Quaternary Complex Formed by Two Cucurbit[7]uril Hosts, Cyclobis(paraquat-*p*-phenylene), and a "Designer" Guest. *Angew. Chem. Int. Ed.* **2016**, *55*, 11507–11511; (b) Ke, C.; Strutt, N. L.; Li. H.; Hou, X.; Hartlieb, K. J.; McGonigal, P. R.; Ma, Z.; Iehl, J.; Stern, C. L.; Cheng, C.; Zhu, Z.; Vermeulen, N. A.; Meade, T. J.; Botros, Y. Y.; Stoddart, J. F.: Pillar[5]arene as a Co-Factor in Templating Rotaxane Formation. *J. Am. Chem. Soc.* **2013**, *135*, 17019–17030; (c) Rekharsky, M. V.; Yamamura, H.; Kawai, M.; Osaka, I.; Arakawa, R.; Sato, A.; Ko, Y. H.; Selvapalam, N.; Kim, K.; Inoue, Y.: Sequential Formation of a Ternary Complex among Dihexylammonium, Cucurbit[6]uril, and Cyclodextrin with Positive Cooperativity. *Org. Lett.* **2006**, *8*, 815–818.

(16) (a) Ooya, T.; Inoue, D.; Choi, H. S.; Kobayashi, Y.; Loethen, S.; Thompson, D. H.; Ko, Y. H.; Kim, K.; Yui, N.: pH-Responsive Movement of Cucurbit[7]uril in a Diblock Polypseudorotaxane Containing Dimethyl α-Cyclodextrin and Cucurbit[7]uril. *Org. Lett.* **2006**, *8*, 3159–3162; (b) Yuan, L.; Wang, R.; Macartney, D. H.: Binding Modes of Cucurbit[6]uril and Cucurbit[7]uril with a Tetracationic Bis(viologen) Guest. *J. Org. Chem.* **2007**, *72*, 4539–4542; (c) Wyman, I. W.; Macartney, D. H.: Host-Guest Complexes and Pseudorotaxanes of Cucurbit[7]uril with Acetylcholinesterase Inhibitors. *J. Org. Chem.* **2009**, *74*, 8031–8038; (d) Sun, H.-L.; Zhang, H.-Y.; Dai, Z.; Han, X.; Liu, Y.: Insights into the Difference Between Rotaxane and Pseudorotaxane. *,Chem. Aisan J.* **2017**, *12*, 265–270; (e) Lin, R.-L.; Li, R.; Shi, H.; Zhang, K.; Meng, D.; Sun, W.-Q.; Chen, K.; Liu, J.-X.: Symmetrical-Tetramethyl-Cucurbit[6]uril-Driven Movement of Cucurbit[7]uril Gives Rise to Heterowheel [4]Pseudorotaxanes. *J. Org. Chem.* **2020**, *85*, 3568–3575.

(17) Olah, G. A.; Farooq, O.; Farnia, S. M. F.; Wu, A.: Aromatic substitution. 58. Boron tris(triflate)-catalyzed adamantylation of benzene and toluene with 1- and 2-haloadamantanes and adamantanoyl chlorides. Isomerization of phenyl- and tolyladamantanes. *J. Org. Chem.* **1990**, *55*, 1516–1522.

(18) Cheng, W. C.; Kurth, M. J.: The Zincke Reaction. A Review. *Org. Prep. Proced. Int.* **2002**, *34*, 585–608.

(19) Rössler, S. L.; Jelier, B. J.; Tripet, P. F.; Shemet, A.; Jeschke, G.; Togni, A.; Carreira, E. E.: Pyridyl Radical Cation for C−H Amination of Arenes. *Angew. Chem. Int. Ed.* **2019**, *58*, 526–531.

(20) Hettiarachchi, D. S. N.; Macartney, D. H.: Cucurbit [7] uril host–guest complexes with cationic bis(4,5-dihydro-1H-imidazol-2-yl) guests in aqueous solution. *Can. J. Chem.* **2006**, *84*, 905−914.

(21) Černochová, J.; Branná, P.; Rouchal, M.; Kulhánek, P.; Kuřitka, I.; Vícha, R.: Determination of Intrinsic Binding Modes by Mass Spectrometry: Gas-Phase Behavior of Adamantylated Bisimidazolium Guests Complexed to Cucurbiturils. *Chem. Eur. J.* **2012**, *18*, 13633–13637.

(22) Sahai, R.; Loper, G. L.; Lin, S. H.; Eyring, H.: Investigation of the Composition and Formation Constant of Molecular Complexes. *Proc. Natl. Acad. Sci. U. S. A.* **1974**, *71*, 1499–1503.

(23) Havemeyer, R. N.: Freezing Point Curve of Dimethyl Sulfoxide—Water Solutions. *J. Pharm. Sci.* **1966**, *55*, 851–853.

(24) Johnson, E. S. in *Advances in Magnetic Resonance*, Vol. 1(Ed.: J. S. Waugh), Academic Press, New York, **1956**, pp. 64–68.

(25) Jeener, J.; Meier, B. H.; Bachmann, P.; Ernst, R. R.: Investigation of exchange processes by two-dimensional NMR spectroscopy. *J. Chem. Phys.* **1979**, *71*, 4546–4553.

(26) (a) Kulkarni, S.; Jelínková, K.; Nečas, M.; Prucková, Z.; Rouchal, M.; Dastychová, L.; Kulhánek, P.; Vícha, R.: A Photochemical/Thermal Switch Based on 4,4′-Bis(benzimidazolio)stilbene: Synthesis and Supramolecular Properties. *ChemPhysChem* **2020**, *21*, 2084–2095. (b) Babjaková, E.; Branná, P.; Kuszyńska, M.; Rouchal, M.; Prucková, Z.; Dastychová, L.; Vícha, J.; Vícha, R.: An adamantane-based disubstituted binding motif with picomolar dissociation constants for cucurbit[n]urils in water and related quaternary assemblies. *RSC Adv.* **2016**, *6*, 105146–105153. (c) Noujeim, N.; Jouvelet, B.; Schmitzer, A. R.: Formation of Inclusion Complexes between 1,1′-Dialkyl-3,3′-(1,4-phenylene)bisimidazolium Dibromide Salts and Cucurbit[7]uril. *J. Phys. Chem. B* **2009**, *113*, 16159–16168. (d) Elie, C.-R.; Noujeim, N.; Pardin, C; Schmitzer, A. R.: Uncovering new properties of imidazolium salts: Cl^- transport and supramolecular regulation of their transmembrane activity. *Chem. Commun.* **2011**, *47*, 1788–1790.

(27) (a) Fokina, N. A.; Tkachenko, B. A.; Dahl, J. E. P.; Carlson, R. M. K.; Fokin, A. A.; Schreiner, P. R.: Synthesis of diamondoid carboxylic acids. *Synthesis* **2012**, *44*, 259–264. (b) Fokina, N. A.; Tkachenko, B. A.; Merz, A.; Serafin, M.; Dahl, J. E. P.; Carlson, R. M. K.; Fokin, A. A.; Schreiner, P. R.: Functionalized nanodiamonds, Part 8. Hydroxy derivatives of diamantane, triamantane, and [121]tetramantane: selective preparation of bis-apical derivatives. *Eur. J. Org. Chem.* **2007**, 4738–4745.

(28) Mosset, P.; Grée, R.: Indium-Catalyzed Friedel–Crafts Alkylation of Monosubstituted Benzenes by 1-Bromoadamantane. *Synlett.* **2013**, 24, 1142–1146.

(29) Rouchal, M.; Matelová, A.; Pires de Carvalho, F.; Bernat, R.; Grbić, G.; Kuřitka, I.; Babinský, M.; Marek, R.; Čmelík, R.; Vícha, R.: Adamantane-bearing benzylamines and benzylamides: novel building blocks for supramolecular systems with finely tuned binding properties towards β-cyclodextrin. *Supramol. Chem.* **2013**, *25*, 349–361.

(30) Mori, S.; Takeuchi, Y.; Tanatani, A.; Kagechika, H.; Fujii, S.: Development of 1,3-diphenyladamantane derivatives as nonsteroidal progesterone receptor antagonists. *Bioorg. Med. Chem.* **2015**, *23*, 803–809.

(31) Vícha, R.; Kuřitka, I.; Rouchal, M.; Ježková, V.; Zijerhut, A.: Directing effects in nitration of 1-adamantyl bearing aromatic ketones. *Arkivoc*, **2009**, (xii), 60–80.

(32) Vícha, R.; Rouchal, M.; Kozubková, Z.; Kuřitka, I.; Marek, R.; Branná, P.; Čmelík, R: Novel Adamantane-Bearing Anilines and Properties of Their Supramolecular Complexes with β-Cyclodextrin. *Supramol. Chem.* **2011**, *23*, 663–677.

(33) (a) Overhauser, A. W.: Polarization of Nuclei in Metals. *Phys. Rev.* **1953**, *92*, 411–415. (b) Kaiser, R.: Use of the Nuclear Overhauser Effect in the Analysis of High-Resolution Nuclear Magnetic Resonance Spectra. *J. Phys. Chem.* **1963**, *39*, 2435–2442. (c) Kaiser, R.: Intermolecular Nuclear Overhauser Effect in Liquid Solutions. *J. Phys. Chem.* **1965**, *42*, 1838–1839. (d) Anet, F. A. L.; Bourn,

A. J. R.: Nuclear Magnetic Resonance Spectral Assignments from Nuclear Overhauser Effects. *J. Am. Chem. Soc.* **1965**, *87*, 5250–5251. (e) Neuhaus, D.; Williamson, M. *The Nuclear Overhauser Effect in Structural and Conformational Analysis*, VCH Publisher, New York, **1989**.

(34) Linden, A.; Mariz, R.; Blumentritt, S.; Dorta, R. *CSD Commun.* **2020**, CCDC Number: 2003919.

(35) (a) CrystalClear. Rigaku Americas, The Woodlands, Texas, USA, and Rigaku Corporation, Tokyo, Japan, **2014**; (b) CrysAlisPro. Rigaku Oxford Diffraction, Oxford, UK, **2015**.

(36) (a) G. M. Sheldrick, *Acta Cryst.* **2015**, *A71*, 3; (b) G. M. Sheldrick, *Acta Cryst.* **2015**, *C71*, 3.

(37) Wang, J.; Wolf, R. M.; Caldwell, J. W.; Kollman, P. A.; Case, D. A.: Case: Development and testing of a general amber force field. *J. Comput. Chem.* **2004**, *25*, 1157–1174.

(38) Kirschner, K. N.; Yongye, A. B.; Tschampel, S. M.; González-Outeiriño, J.; Daniels, C. R.; Foley, B. L.; Woods, R. J.: GLYCAM06: a generalizable biomolecular force field. Carbohydrates. *J. Comput. Chem.* **2008**, *29*, 622–655.

(39) Case, D. A.; Betz, R. M.; Botello-Smith, W.; Cerutti, D. S.; Cheatham III, T. E.; Darden, T. A.; Duke, R. E.; Giese, T. J.; Gohlke, H.; Goetz, A. W.; *et al. AMBER 16*. University of California: San Francisco, **2016**.

(40) (a) Comer, J.; Gumbart, J. C.; Hénin, J.; Lelièvre, T.; Pohorille, A.; Chipot, C.: The Adaptive Biasing Force Method: Everything You Always Wanted To Know but Were Afraid To Ask. *J. Phys. Chem. B* **2015**, *119*, 1129–1151. (b) Darve, E.; Rodriguez-Gómez, D.; Pohorille, A.: Adaptive biasing force method for scalar and vector free energy calculations. *J. Chem. Phys.* **2008**, *128*, 144120/1–13.

(41) (a) Raiteri, P.; Laio, A.; Gervasio, F. L; Micheletti, C.; Parrinelo, M.: Efficient Reconstruction of Complex Free Energy Landscapes by Multiple Walkers Metadynamics. *J. Phys. Chem. B* **2006**, *110*, 3533–3539. (b) Minoukadeh, K.; Chipot, C.; Lelièvre, T.: Potential of Mean Force Calculations: A Multiple-Walker Adaptive Biasing Force Approach. *J. Chem. Theory. Comput.* **2010**, *6*, 1008–1017.

(42) Kulhánek, P.; Štěpán, J.; Fuxreiter, M.; Mones, L.; Střelcová, Z.; Petřek, M.: PMFLib – A Toolkit for Free Energy Calculations https://github.com/kulhanek/pmflib.

(43) Mones, L.; Bernstein, N.; Csányi, G.: Exploration, Sampling, And Reconstruction of Free Energy Surfaces with Gaussian Process Regression. *J. Chem. Theory Comput.* **2016**, *12*, 5100–5110.

(44) Stetter, H.; Schwartz, M.; Hirschhorn, A.: Über Verbindungen mit Urotropin-Struktur, XII. Monofunktionelle Adamantan-Derivate. *Chem. Ber.* **1959**, *92*, 1629–1635.

(45) (a) Matsubara, K.; Ishibashi, T.; Koga, Y: C−F Bond-Cleavage Reactions of Fluoroalkanes with Magnesium Reagents and without Metal Catalysts. *Org. Lett.* **2009**, *11*, 1765–1768; (b) Chalais, S.; Cornélis, A.; Gerstmans, A.; Kołodziejski, W.; Laszlo, P.; Mathy, A.; Métra P.: Direct Clay-Catalyzed Friedel–Crafts Arylation and Chlorination of the Hydrocarbon Adamantane. *Helv. Acta* **1985**, *68*, 1196–1203.

(46) Stepanov, F. N.; Dikolenko, E. I.; Danilenko, G. I.: Adamantane and its derivatives. VI. Substitution reactions in aryladamantanes. *Zh. Obshch. Khim.* **1966**, *2*, 640–643.

(47) Kogay, B. E.; Sokolenko, W. A.: Reactions of 1.3-dehydroadamantane (3.3.1-propellane system) with ch- and nh-acids. *Tetrahedron Lett.* **1983**, *24*, 613–616.

(48) Stringer, B.; Quan, L.;Barnard, P.; Wilson, D.; Hogan, C.: Iridium Complexes of N-Heterocyclic Carbene Ligands: Investigation into the Energetic Requirements for Efficient Electrogenerated Chemiluminescence. *Organometallics* **2014**, *33*, 4860–4872.

(49) Song, Y.; Huang, X.; Hua, H.; Wang, Q.: The synthesis of a rigid conjugated viologen and its cucurbituril pseudorotaxanes. *Dyes Pigm.* **2017**, *137*, 229–235.